A STUDY OF THE EFFECTS OF STRAIN AMPLITUDE AND ENVIRONMENT ON THE MECHANISM OF FATIGUE CRACK INITIATION IN NICKEL

By

JOSEF ANTONIN FILA

Bachelor of Science in Mechanical Engineering

Oklahoma State University

Stillwater, Oklahoma

1978

Submitted to the Faculty of the Graduate College
of the Oklahoma State University
in partial fulfillment of the requirements
for the Degree of
MASTER OF SCIENCE
May, 1978

A STUDY OF THE EFFECTS OF STRAIN AMPLITUDE AND ENVIRONMENT ON THE MECHANISM OF FATIGUE CRACK INITIATION IN NICKEL

Thesis Approved:

C E Price
Thesis Adviser

R L Lowery

A E Kelly

W A Boyd

Norman N Durham
Dean of the Graduate College

ACKNOWLEDGMENTS

The aid of those who helped during this study is gratefully acknowledged. I express my appreciation to Dr. C. E. Price, my major adviser, for his advice, instruction, and encouragement during my graduate study. My thanks are extended to Drs. Richard L. Lowery, Allen E. Kelly, and Donald E. Boyd for serving on my committee.

The School of Mechanical and Aerospace Engineering provided a graduate assistantship which helped to make my graduate study possible.

I would like to thank my parents, Dr. and Mrs. Ladislaus J. Fila, for their moral support and financial aid.

TABLE OF CONTENTS

LIST OF TABLES

LIST OF FIGURES

CHAPTER I

INTRODUCTION

Designers have been troubled by fatigue failures for over a century. A product that is designed for cyclic loading may withstand the loads initially, only to fail after a number of loading cycles. As most products undergo a cyclic loading procedure, fatigue can be a common engineering failure. Fatigue follows cyclic plastic deformation and failures are known to develop from loads less than the nominal yield stress because of localized yielding of individual grains. In order to avoid this problem, designers have, in the past, overdesigned their product. In many instances, however, overdesign is unacceptable. In transportation vehicles such as trucks, trains, and aircraft, overdesign results in an addition of weight to the structure which lowers the payload capacity. Addition of material to lower the stress also means an additional cost to the product. As an alternative, research has increased so that the mechanism leading to failure can be understood.

Objective

The objective of this study will be to test the hypothesis that different strain amplitudes and environments primarily affect the rate of crack initiation rather than the mechanism. The surface condition will be monitored by microhardness indentation and with optical and electron microscopy.

The microhardness measurements of the surface zone will be used to:

1. Determine whether the surface zone hardness reaches a limiting value independent of environment and strain amplitude.

2. Determine whether the surface zone hardness reaches a critical value during crack initiation independent of environment and strain amplitude.

3. Determine whether the surface zone hardness varies with depth in the saturation zone.

Microscopic observation will be used to determine the characteristics of the surface deterioration.

The material to be used is nickel, a face-centered cubic (FCC) metal.

CHAPTER II

REVIEW OF LITERATURE

The fatigue failure sequence is considered to be threefold, consisting of crack initiation, stage I crack propagation, and stage II crack propagation. Most of the research in fatigue has been on the crack propagation and fractography. Recently, the crack initiation process has received more attention. Emphasis in this study is on the mechanism of crack initiation. Comprehensive articles on fatigue by Thompson and Wadsworth (1), Laird and Duquette (2), and Grosskreutz (3) (4) were used as general references.

Crack Initiation

The specimen surface is the origin of almost all fatigue cracks. The stresses there tend to be higher because of bending moments, inhomogeneities, stress concentration from surface finishes, and environmental corrosion effects (5). In rare cases, subsurface fatigue cracks form at internal discontinuities.

Crack initiation starts with strain hardening/softening of the surface. Initially hard and strong materials were found to strain soften and initially soft materials would strain harden. This process is related to the dislocation substructure (6). Materials with a high stacking fault energy have a unique saturation hardness that does not depend on initial surface condition, due to enhanced cross slip. Annealing the

specimen before saturation hardening was found to postpone the formation of slip bands (7). Slip bands are formed during nonhardening strain cycling. With the formation of slip bands, sharp ridges and troughs develop. These are free surface terminations of dense bands of highly localized slip called extrusions and intrusions. It is thought that these cyclically soften compared to the matrix resulting in a plastic strain concentration. These are then called persistent slip bands and are the nuclei of cracks. If the surface is polished and cycled again, slip will occur and congregate at the old persistent slip band location. Alden and Backofen (7) found that the fatigue could be prolonged in aluminum single crystals by using an anodic surface film and repolishing when film cracks were first noted. Fatigue cracks will initiate along slip bands in FCC materials as grain boundary cracking is discouraged by the multiple slip systems of the FCC crystal.

Kramer (8) has suggested an alternative mechanism for initiation of cracks. Here a surface layer of high dislocation density is formed and becomes strong enough to support a dislocation pileup. A crack is then thought to have been triggered from the pileup's resulting stress concentration. Kramer has found that the strength of this layer is independent of strain amplitude and environment, although they do affect the rate at which initiation occurs. The electropolishing of the surface to get a prolonged life is also accepted by Kramer's model as the critical surface layer would be removed. Kramer has used aluminun, titanium, and steel as sample materials.

Crack Propagation

Fatigue cracks that start in slip bands continue to grow on the slip

plane that has the highest resolved shear stress (4). This is the stage I crack propagation. In lower strain amplitudes, stage I accounts for deep crack propagation. Stage II begins when the stage I crack reaches a critical length. The direction of stage II is normal to the tensile stress axis. In a polycrystalline material, stage I propagation connects individual slip band cracks to form a large crack when stage II propagation takes over.

Factors Affecting Fatigue Life

Fatigue life will depend on many factors including strain amplitude, temperature, and corrosive environment. Strain amplitude will govern the fraction of the fatigue life spent in each of crack initiation, crystallographic crack propagation, and noncrystallographic crack propagation. In low cycle fatigue, the crack is initiated very early and most of the propagation is done by the stage II process. In high cycle fatigue, stage I crack propagation is the dominant feature with stage II crack propagation occurring just before fracture.

Temperature can vary the crack initiation stage. Lower temperatures seem to have the same effect as lowering the stacking fault energy. Increase in temperature enhances slip. However, as the temperature reaches one-half the material melting temperature, the site for crack initiation is switched to grain boundaries and voids will be formed at the grain boundary. Little is known about the effect of temperature on crack propagation.

Corrosion fatigue is a combined action of corrosion and cyclic strain. The effect on the surface is greater than the sum of the two acting separately. Many fatigue failures are more correctly corrosion

fatigue failures as moisture in the air is considered a corrosive agent. Results from testing in a vacuum have been found to be much improved over the air environment. Corrosion is very time sensitive in that the sample tested at the same strain level would have a shorter life if the frequency of cycling was reduced (9).

In aqueous solutions, corrosion is known to affect the fatigue crack initiation. Several mechanisms were reviewed by Duquette (10) and in more depth by Laird and Duquette (2). Many mechanisms have been suggested including stress concentration formed at corrosion pits, lowering the surface energy of the metal by absorption and the propagation of microcracks, and the dissolution by electrochemical means of obstacles that would inhibit slip. No working model exists, as most proposed mechanisms have a few major discrepancies.

CHAPTER III

THE APPROACH

Fatigue tests were done with a commercially pure nickel, Inco material Nickel 200. The specimens were designed so that the location of the fracture would be the same for all tests because of a strain amplitude gradient along the gage length. The specimens were electropolished to remove all surface effects of mechanical polishing. Vacuum annealing was done to thermal-etch the specimens and to achieve the material's softest state. Specimens were then fatigued by controlled cyclic strain in fully reversed bending. The fatigue tests were as follows:

1. Seven samples were tested in a dry air atmosphere at strain amplitudes to give fatigue lives at 10^3 to 10^7 cycles.

2. Seven samples were tested in a 2 percent Nitric acid aqueous atmosphere at the strain amplitudes that were used for the dry air environment.

From these tests, data from the two environments at the same strain amplitude were compared to determine the effects of environment. The effect of strain amplitude was evaluated for each environment.

The data for the above comparisons consist of:

1. Surface hardness profiles. Hardness readings were taken along the gage length of the sample at two different surface depths for all samples.

2. Optical microscope observations. Observations and photographs

were recorded along the gage length. The optical microscope was used to observe slip bands inthe grains and the surface deterioration at the fracture edge.

3. Scanning electron microscope observations. Photographs were made of selected specimens to find the fatigue cracks.

4. S-N Curve. This was compiled from the fatigue tests to compare the life required to break a specimen of each environment at a given strain level.

One specimen was electropolished after fatigue failure to observe the persistent slip bands and fatigue cracks.

CHAPTER IV

EXPERIMENTAL PROCEDURE

The Material

Inco Nickel 200 is a commercially pure nickel. In practical application, it is used in corrosive environments and elevated temperatures. Nickel 200 has these advantages for this study:

1. Nickel has a relatively high strain hardening capacity so that large hardness changes are possible.

2. Nickel has an ideal hardness ($H_V \approx 80$ kg mm^{-2}) so that a large range of loads and therefore indent depths can be made with the microhardness machine. The indents have been found to be easy to read after fatigue surface deterioration at medium to high loads.

3. Nickel 200 is weak enough so that specimens could be broken by available equipment.

4. Nickel has a high stacking fault energy which refers to the ease of cross slip. Materials with a high stacking fault energy have a unique stress-strain curve.

5. Nickel 200 is a face-centered cubic metal making it easy to observe slip in grains. Nickel is also an FCC metal that has not been overstudied (such as copper and aluminum).

As received, the Ni200 was in cold rolled annealed plate from Huntington Alloy heat number N96564. The supplied chemical analysis and mechanical properties determined by Kreiner (11) are presented in Table

TABLE I

PROPERTIES OF NICKEL 200

(A) CHEMICAL COMPOSITION

HUNTINGTON ALLOYS HEAT NO. N9656A

ELEMENT	PER CENT
NICKEL (PLUS COBALT)	99.60
COPPER	.01
IRON	.04
MANGANESE	.24
CARBON	.05
SILICON	.01
SULFUR	.005

(B) MECHANICAL PROPERTIES

ELASTIC MODULUS

186.94 GPA 27,110 KSI

CYCLIC STRAIN HARDENING EXPONENT

.118

CYCLIC STRENGTH COEFFICIENT

661.92 MPA 96.0 KSI

I. After mechanically polishing, electropolishing, and vacuum-annealing the grain diameter was 100 to 200μ.

Experimental Techniques

Specimen Design

The specimens were made as shown in Figure 1. When displaced at the "free" end, the nominal stress gradient is as shown in Figure 2. The nominal stress (σ_n) is defined as the cyclic strain amplitude (ε_a), multiplied by the elastic modulus (E).

$$\sigma_n = E \cdot \varepsilon_a.$$

According to beam theory, the nominal stress at the narrow part of the tapered section was the maximum for the specimen. Maximum nominal stress depended on the displacement of the "free end" (y_e).

$$\sigma_n = K \cdot y_e;\ K = 41.07\ \text{MPa mm}^{-1}$$

Strain gages were used to check the stress level and to make corrections for a concentration factor. Tests showed this was not necessary and the above stress equation was satisfactory.

The goemetry was chosen so that a smooth gradient of strain was produced along the gage length. The gage length refers to the section of the sample where the width has been reduced. The length of the gage area was made short enough so that the samples would break at the same location. The sample width was limited by the specimen size accepted by the scanning electron microscope and was chosen so that all samples could be machined from the same plate of raw material.

Figure 1. Sample Geometry

FRONT VIEW

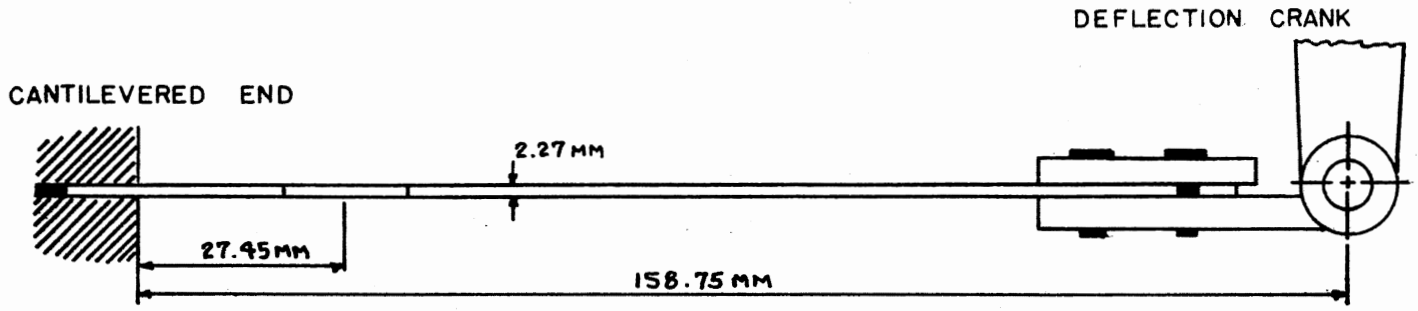

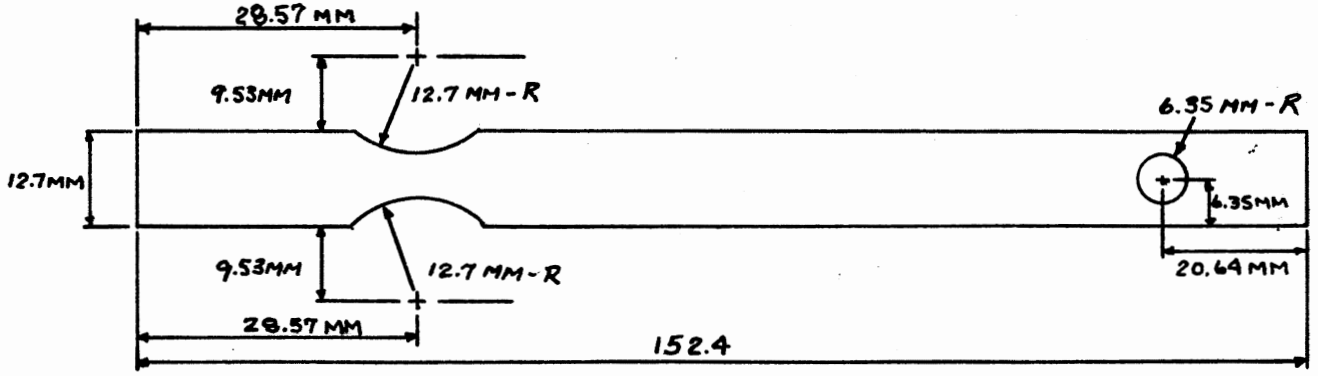

TOP VIEW

Figure 2. Stress Profile Along the Gage Length. Stresses were calculated assuming elastic behavior. It is recognized that this is not the case above 300 MPa.

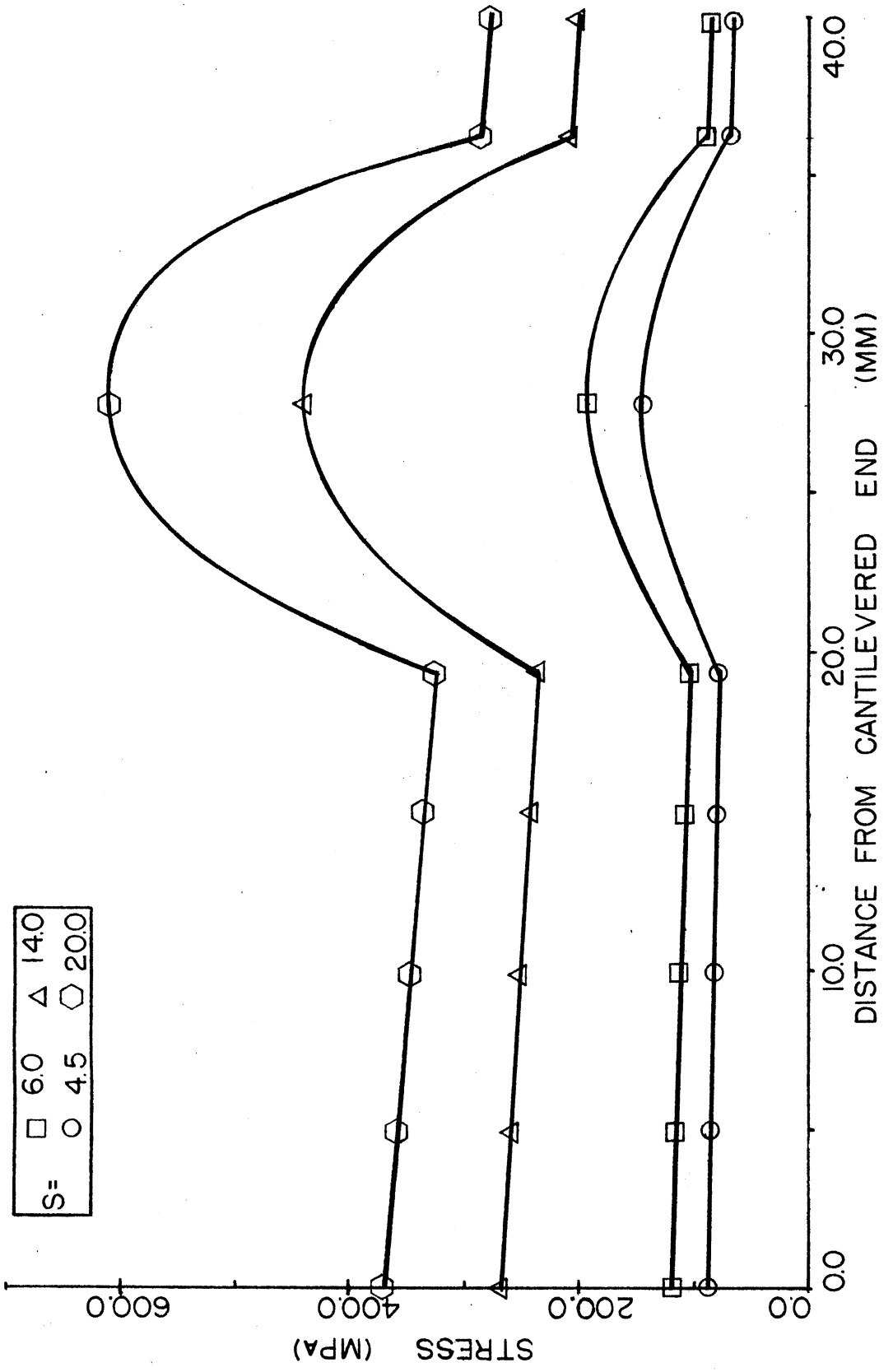
STRESS (MPA)
600.0
400.0
200.0
0.0
0.0
10.0
20.0
30.0
40.0
DISTANCE FROM CANTILEVERED END (MM)
S= □ 6.0 △ 14.0
○ 4.5 ⬡ 20.0

Specimen Preparation

The specimens were received with a rolled and pickled surface. Both sides were mechanically polished to remove all surface pits. Final polishing was done with levigated alumina. The samples were then cleaned in a Buehler Ltd. 75-1950 Ultrasonic Cleaner with ethyl alcohol. This was done to remove all alumina from the specimen surface that might cause pits during the electropolishing process. Specimens were then electropolished with a Buehler Ltd. 70-1721 AB Electropolisher using the method of Tegart (12) and Beland (13). The solution used was 57 percent sulfuric acid in distilled water. Polishing time was 300 seconds with a nickel foil cathode, at a current density of 0.4 Acm^{-2}. Specimens were annealed in a mild vacuum ($\approx$26.66 Pa) at 750°C for one hour and oven-cooled. Thermal etching was done to reveal the grain structure. Hardness readings of all samples were made after annealing.

The dry air environment was provided by means of an asbestos cloth tape which held a layer of anhydrous calcium sulfate to the specimen surface. The gage length was then wrapped in a polyvinylidene chloride sheet several times and secured with rubber bands. The nitric acid environment was made by wrapping a thin layer of cotton around the gage length and saturating the cotton with the acid solution. This was wrapped with plastic sheeting like the dry air specimen. This method of environments is similar to that of Nichols and Rostoker (12). A nitric acid solution was chosen as it is an active corrosive environment for nickel.

Fatigue Testing

Fatigue testing was done on a Budd VSP-150 variable plate machine in full reversed bending. The speed of the cycling was 35 Hz. This was chosen as it is in the neighborhood of the applied frequencies used in industry. The machine varied deflection by an eccentric crank. The settings for the deflections on the machine are those listed as stress setting in the hardness profiles. During the tests a strobe light was used to check the cyclic frequency and the deflected profile as in Figure 3.

Microhardness Testing

The Vickers Diamond Pyramid Hardness test was used for all microhardness readings. As the diamond indenter produces geometrically similar indents for different loads, the hardness value is considered to be independent of load. The Vickers hardness value is found by the equation:

$$H_v = \frac{\text{Load}}{\text{Contact Area}} = \frac{1.854\ W}{d^2}\ \text{kg mm}^{-2}$$

where W is the load applied, and d is the mean diagonal length. Indent depth is approximately 0.15 d. All following hardness values are in consistent units of kg mm^{-2}.

Initial hardness readings were taken at three different loads: 5, 50, and 500 g. Sample indents are shown in Figure 4. The higher load indents were much easier to measure and the standard deviation was under five units of hardness. The least load indent diagonals were very difficult to measure precisely and as a result, the standard deviation was over ten units of hardness. After a preliminary test sample failure, it

Figure 3. Fatigue Test Apparatus. Specimen profile is viewed at maximum deflection during fatigue test. The gage of the sample is covered with the environment wrap

Figure 4. Microhardness Indents in Nickel. Diamond pyramid hardness indents were made on a sample after fatigue testing. The indents were made with indent loads from 5 g to 500 g (X380)

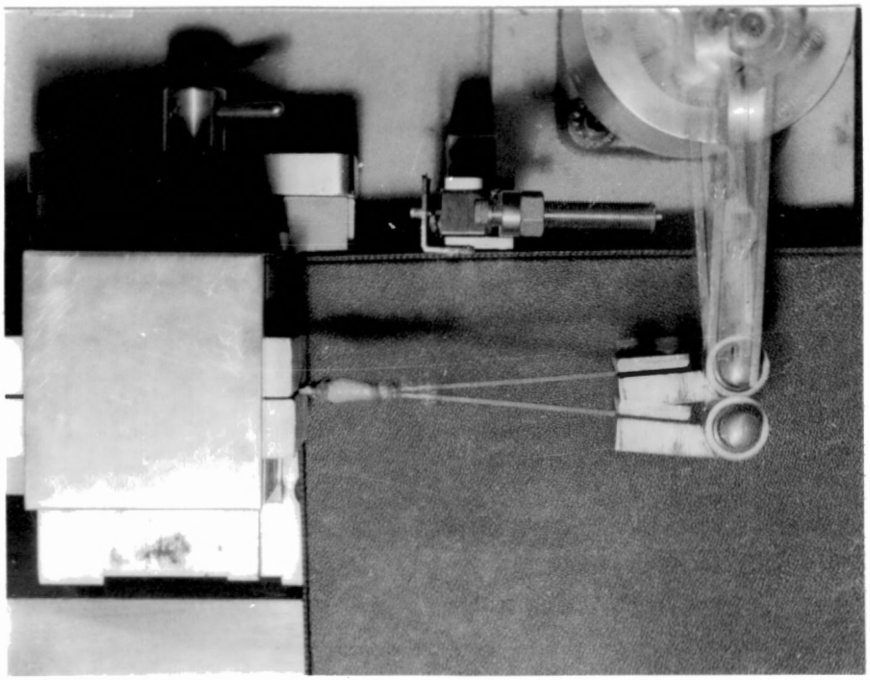

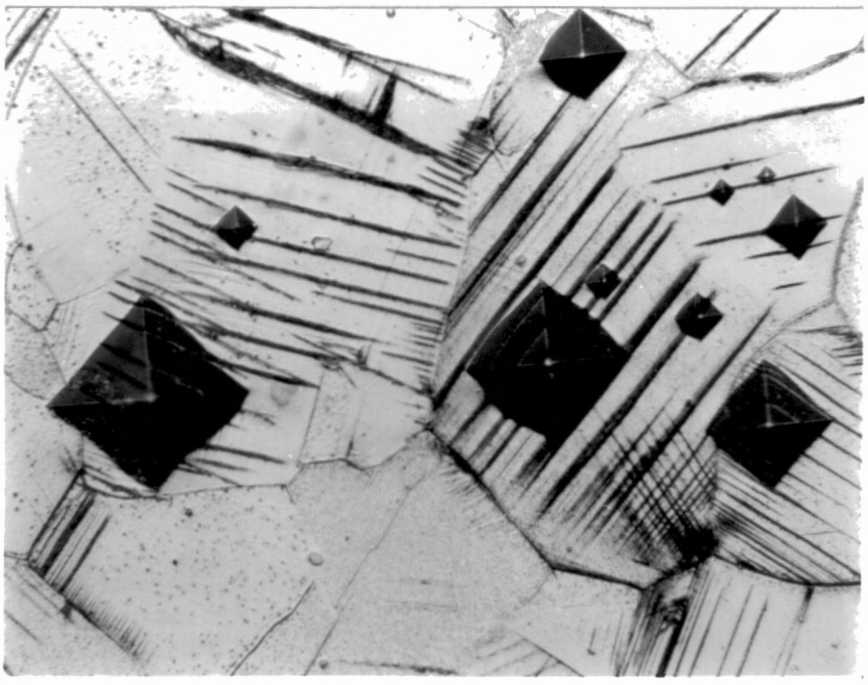

was found that the surface deterioration was often too great to get consistent hardnesses at the lowest load. This test load was eliminated and tests were made with the 50 and 500 g loads.

The mean initial hardness was H_V = 103.45 for the 50 g load and H_V = 92.41 for the 500 g load. This was consistent with earlier readings.

After failure, hardness measurements were made along the gage length. The indents were made in the middle of grains as much as possible. Many indents were made within three millimeters of the crack edge so that maximum hardness could be found. A Leitz Miniload microhardness tester was used for hardness readings.

Microscopic Observations

The optical microscope was used to observe all samples after failure in order to check the extent of surface distortion near the fracture edge, the surface deterioration in the acid environments, and the presence of slip in grains along the gage length. Samples were ultrasonically cleaned before observations were made. It was found that the Reichert N. 312527 Microscope was more effective with Normarski interference contrast equipment. This gave the surface a sense of depth. Surface distortion and slip lines were much easier to observe with this equipment.

The JEOL-35 scanning electron microscope (SEM) observations were made to find the kind of cracking near the fracture (i.e., crystallographic, noncrystallographic) and the initial stage of cracks among the slip lines on the gage length away from the fracture edge. The optical microscope was used primarily to view the surface deterioration and the

first appearance of slip lines. These areas of interest were then observed in the scanning electron microscope up to 4000x in order to locate incipient cracks.

CHAPTER V

EXPERIMENTAL RESULTS

Results

After the various data were collected from the fatigue tests, microhardness measurements, and surface observations, the following results were found:

1. The different environments had effects on fatigue life. The data are presented in the form of a nominal-stress versus cycles-to-failure (S-N) diagram shown in Figure 5.

2. Surface hardness varies along the gage length of the specimen. Plots of surface hardness data values are presented in Figures 10 through 22.

3. Surface deterioration was observed by optical microscopy and was found to vary for different strain amplitudes and environments.

4. Surface cracks were observed in some selected samples by use of the scanning electron microscope.

Samples tested in the nitric acid environment had much shorter lives than those tested in dry air for low strain amplitude, Figure 5. At very high strain amplitudes there was very little difference in fatigue life. A tabular form of fatigue life data is given in Table II. It is noted that four data points are presented at a nominal stress of 259.4 MPa. The middle points, which seem to deviate from the curve of the other points, were the first samples tested. Both showed some evidence that

Figure 5. S-N Curves for Tested Samples

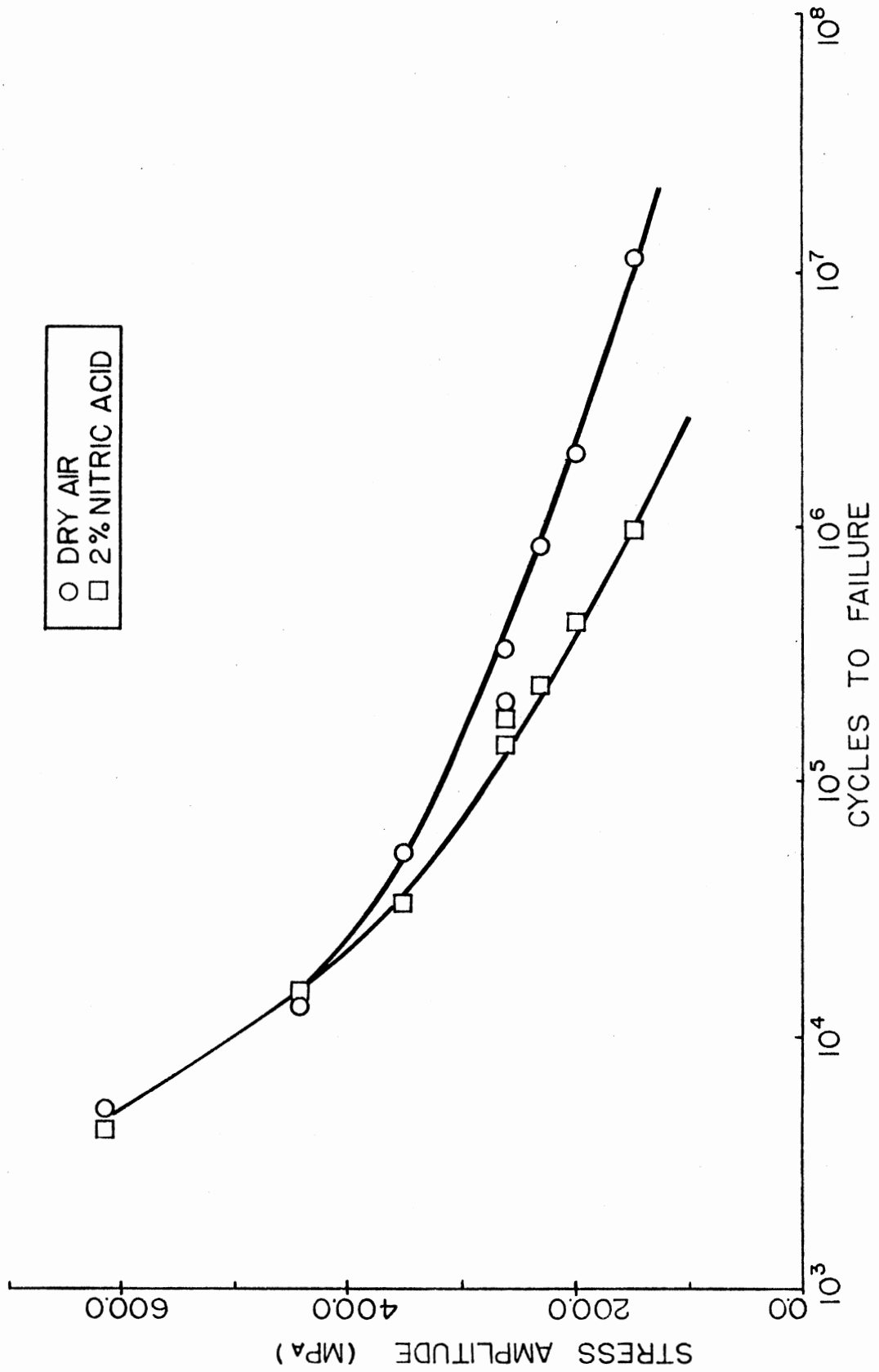
O DRY AIR
□ 2% NITRIC ACID
STRESS AMPLITUDE (MPa)
0.0
200.0
400.0
600.0
10^3
10^4
10^5
10^6
10^7
10^8
CYCLES TO FAILURE

TABLE II

FATIGUE TEST DATA

STRESS SETTING S	NOMINAL STRESS MPA	KSI	FATIGUE LIFE	ENVIRONMENT	SAMPLE
4.5	146.9	21.31	11,557,600	DRY AIR	4A
4.5	146.9	21.31	968,600	ACID	2B
6.0	195.4	28.34	2,031,700	DRY AIR	3B
6.0	195.4	28.34	421,750	ACID	8B
7.0	227.5	33.00	856,900	DRY AIR	6B
7.0	227.5	33.00	235,000	ACID	7B
8.0	259.4	37.62	330,200	DRY AIR	10B
8.0	259.4	37.62	194,600	DRY AIR	1A
8.0	259.4	37.62	180,000	ACID	6A
8.0	259.4	37.62	144,900	ACID	5A
11.0	353.3	51.40	51,400	DRY AIR	2A
11.0	353.3	51.40	31,100	ACID	7A
14.0	444.1	64.41	13,400	DRY AIR	3A
14.0	444.1	64.41	16,600	ACID	1B
20.0	613.1	88.92	5,200	DRY AIR	5B
20.0	613.1	88.92	4,400	ACID	9B

pure bending did not occur. The fatigue machine was adjusted after those tests to insure pure bending and then those strain amplitude tests were repeated.

Hardness profiles were done along the gage length of each sample. These are presented in Figures 10 through 22. The legend for interpreting all hardness profiles is given in Figure 6. Observations of these profiles led to recognition of several trends. Hardness values were found to vary along the gage length, which is explained by the nominal stress gradient in Figure 2.

Superposition of the hardness profiles facilitated an observation that at the same strain amplitude and indent load, the surface hardness profiles of the two environments were almost identical. Examples of this for an indent load of 50 g are given in Figure 7 for a low strain amplitude and in Figure 8 for a high strain amplitude.

In all hardness profiles the maximum surface hardness was found at the fracture edge. The hardness value then decreased as distance from the edge increased. This is somewhat different from the copper results of Davies (16) where the fracture edge had softened by a recovery process after fatigue. There was no suggestion of recovery in this study. The maximum surface hardness for all profiles was $H_V \approx 160\text{-}165$. This limiting value was found to be constant for all strain amplitudes in both test environments and for both indent loads, which may be observed in Figures 10 through 22. At low strain amplitudes this value was found at the fracture edge, while at high strain amplitudes the maximum value was found along most of the gage length. This can be seen in Figure 9 for a 50 g indent load.

Figure 6. Legend for Surface Hardness Profiles

S= (A) (B)
NF= (C)

(A) NOMINAL STRESS

SETTING STRESS

S	MPA	KSI
4.5	146.95	21.31
6.0	195.45	28.34
7.0	227.54	33.00
8.0	259.40	37.62
11.0	353.33	51.40
14.0	444.12	64.41
20.0	613.12	88.92

(B) SAMPLE ENVIRONMENT

DA - DRY AIR
AC - 2% NITRIC ACID SOLUTION

(C) SAMPLE LIFE

NF - NUMBER OF CYCLES TO FAILURE

HARDNESS PROFILES

FIGURE

HARDNESS LOAD - 50 GRAMS

FIGURE

HARDNESS LOAD

○ - 50 GRAMS

□ - 500 GRAMS

Figure 7. Surface Hardness Profiles of Samples 4A and 2B

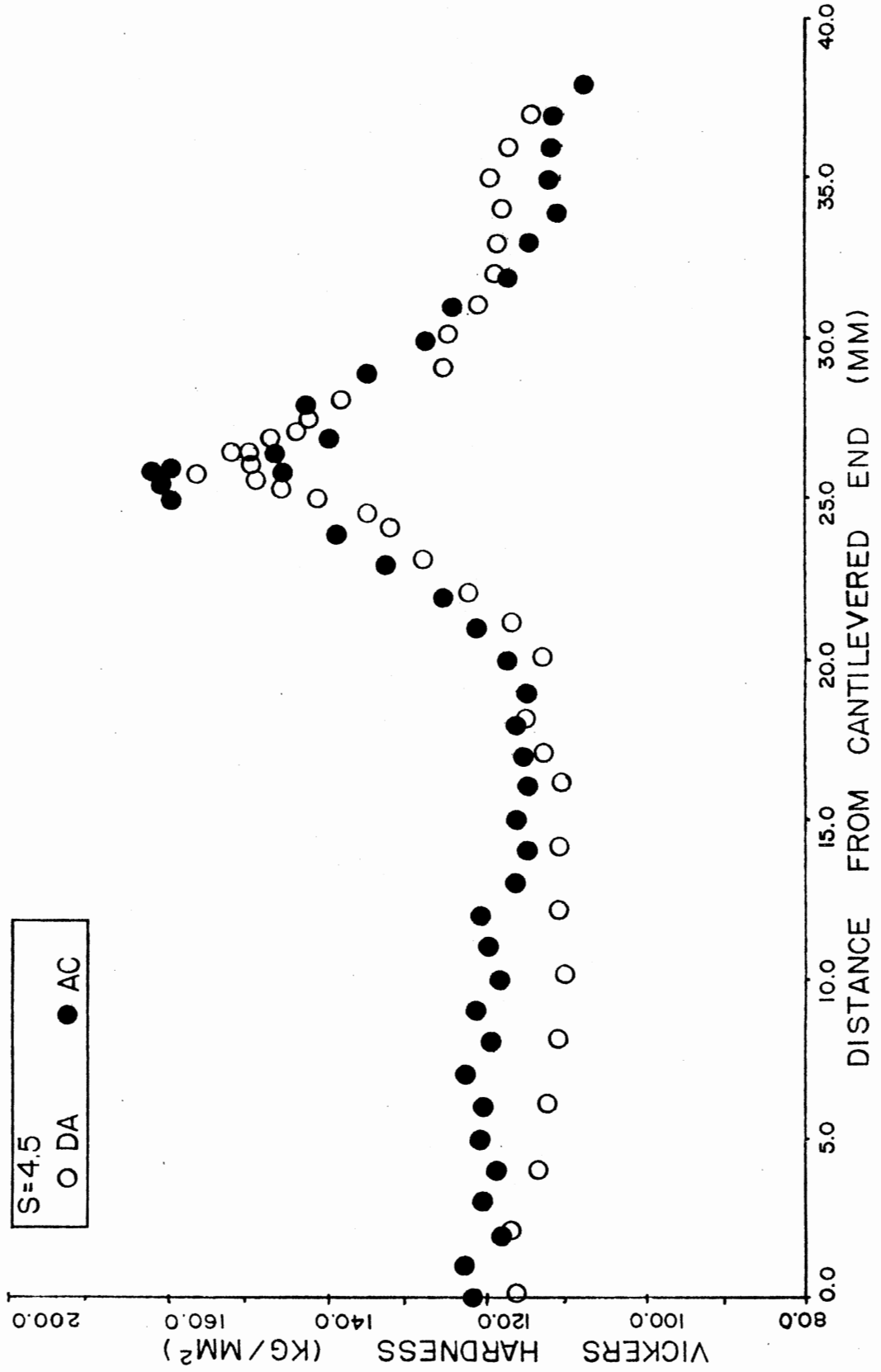
S=4.5
O DA
● AC
VICKERS HARDNESS (KG/MM²)
80.0
100.0
120.0
140.0
160.0
200.0
0.0
5.0
10.0
15.0
20.0
25.0
30.0
35.0
40.0
DISTANCE FROM CANTILEVERED END (MM)

Figure 8. Surface Hardness Profiles of Samples 3A and 1B

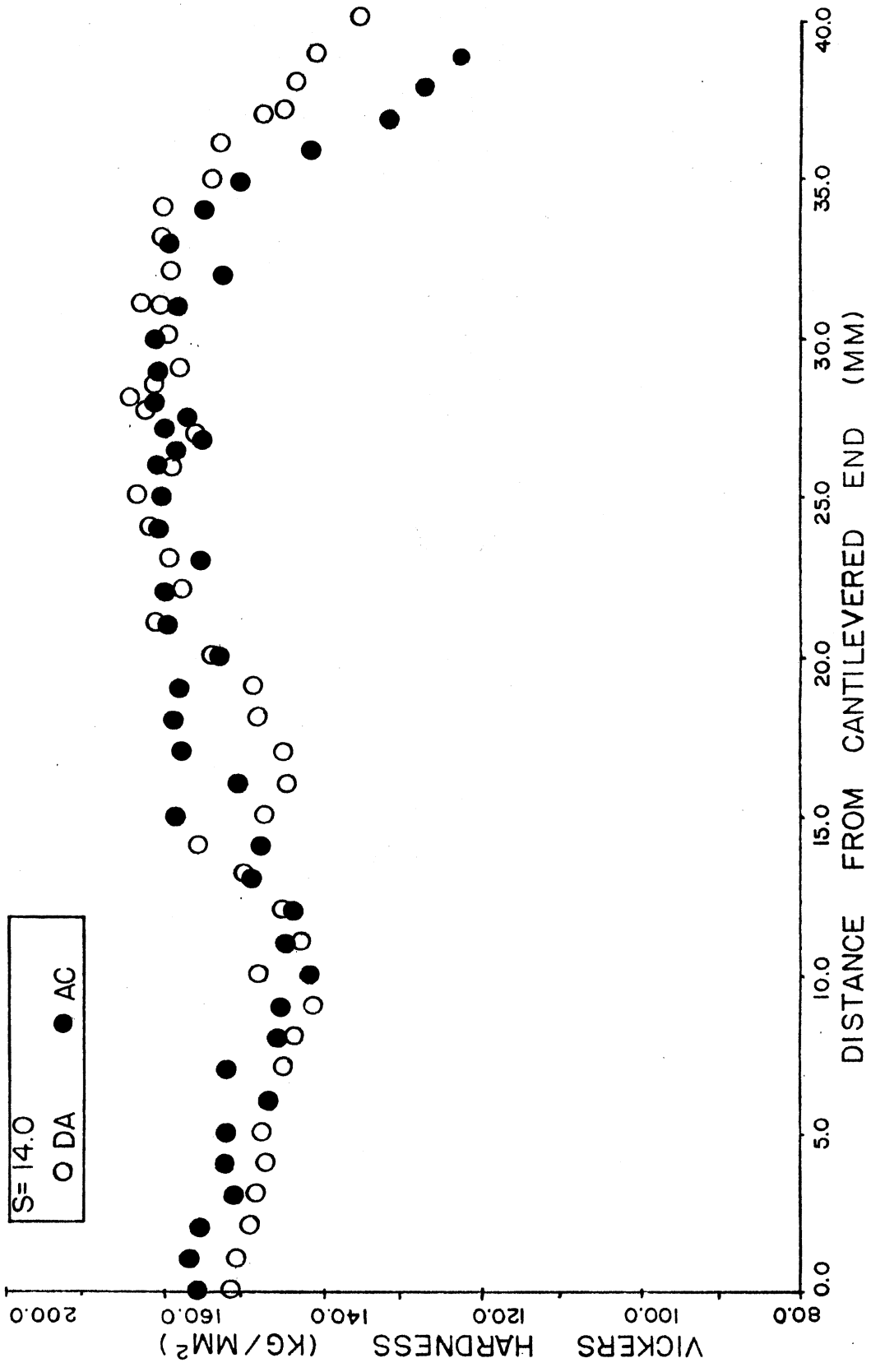
S= 14.0
O DA
● AC
VICKERS HARDNESS (KG/MM²)
80.0
100.0
120.0
140.0
160.0
200.0
0.0
5.0
10.0
15.0
20.0
25.0
30.0
35.0
40.0
DISTANCE FROM CANTILEVERED END (MM)

Figure 9. Surface Hardness Profile Comparison

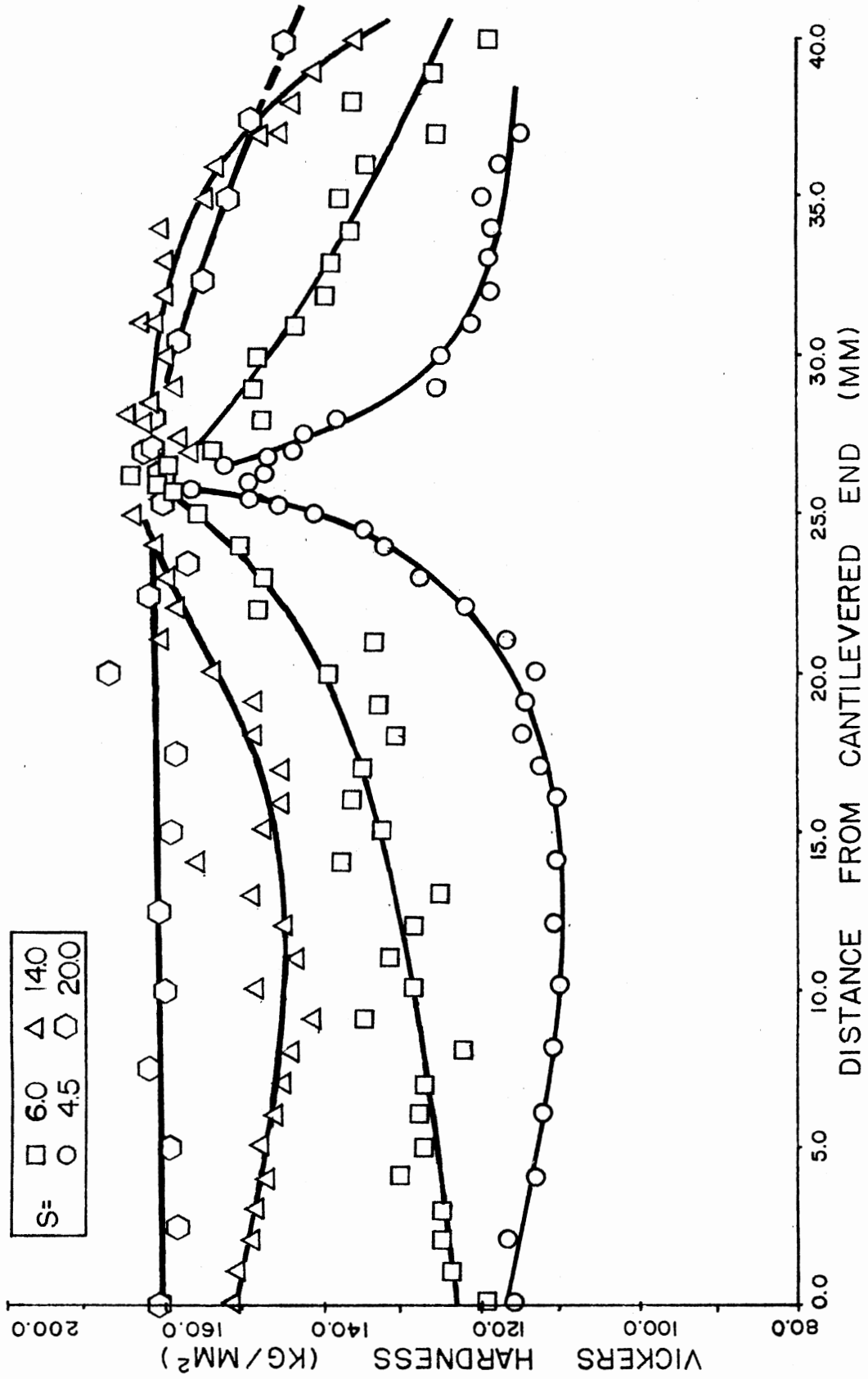
VICKERS HARDNESS (KG/MM²)
80.0
100.0
120.0
140.0
160.0
200.0
0.0
5.0
10.0
15.0
20.0
25.0
30.0
35.0
40.0
DISTANCE FROM CANTILEVERED END (MM)
S= □ 6.0 △ 14.0
○ 4.5 ⬡ 20.0

Figure 10. Surface Hardness Profile of Sample 4A

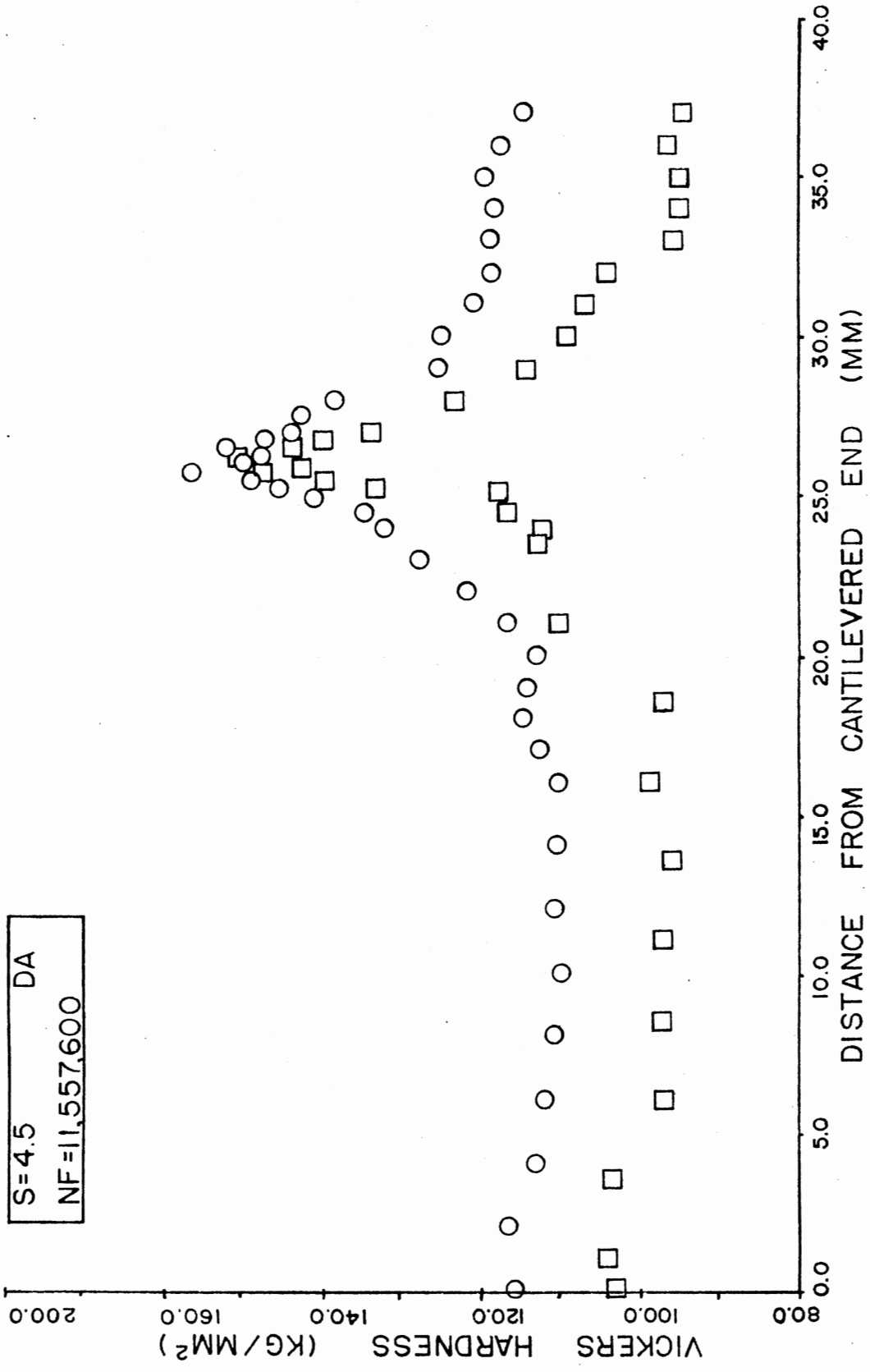
S=4.5 DA
NF=11,557,600
VICKERS HARDNESS (KG/MM²)
80.0
100.0
120.0
140.0
160.0
200.0
0.0
5.0
10.0
15.0
20.0
25.0
30.0
35.0
40.0
DISTANCE FROM CANTILEVERED END (MM)

Figure 11. Surface Hardness Profile of Sample 2B

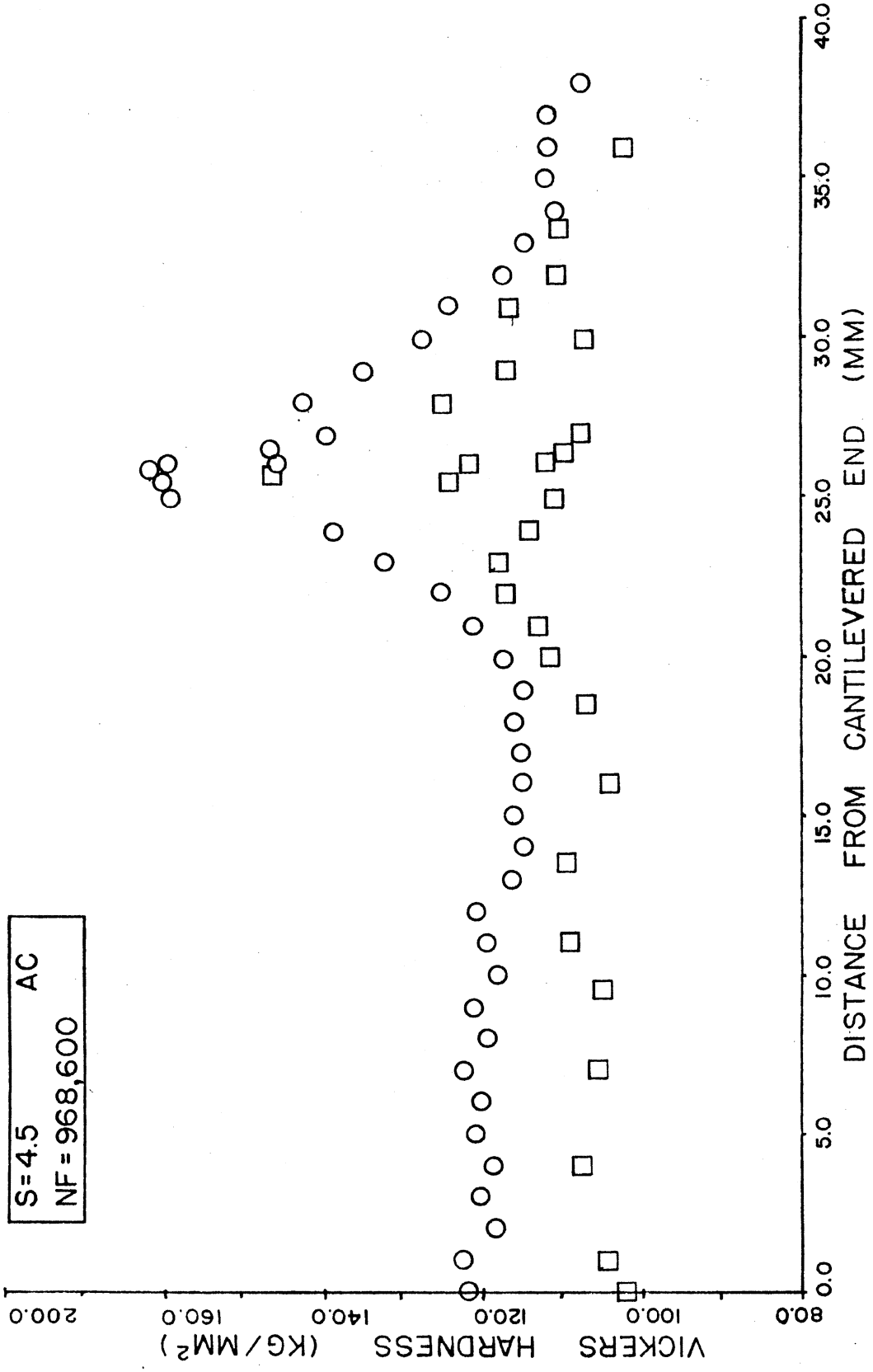
S=4.5 AC
NF=968,600
VICKERS HARDNESS (KG/MM²)
80.0
100.0
120.0
140.0
160.0
200.0
0.0
5.0
10.0
15.0
20.0
25.0
30.0
35.0
40.0
DISTANCE FROM CANTILEVERED END (MM)

Figure 12. Surface Hardness Profile of Sample 3B

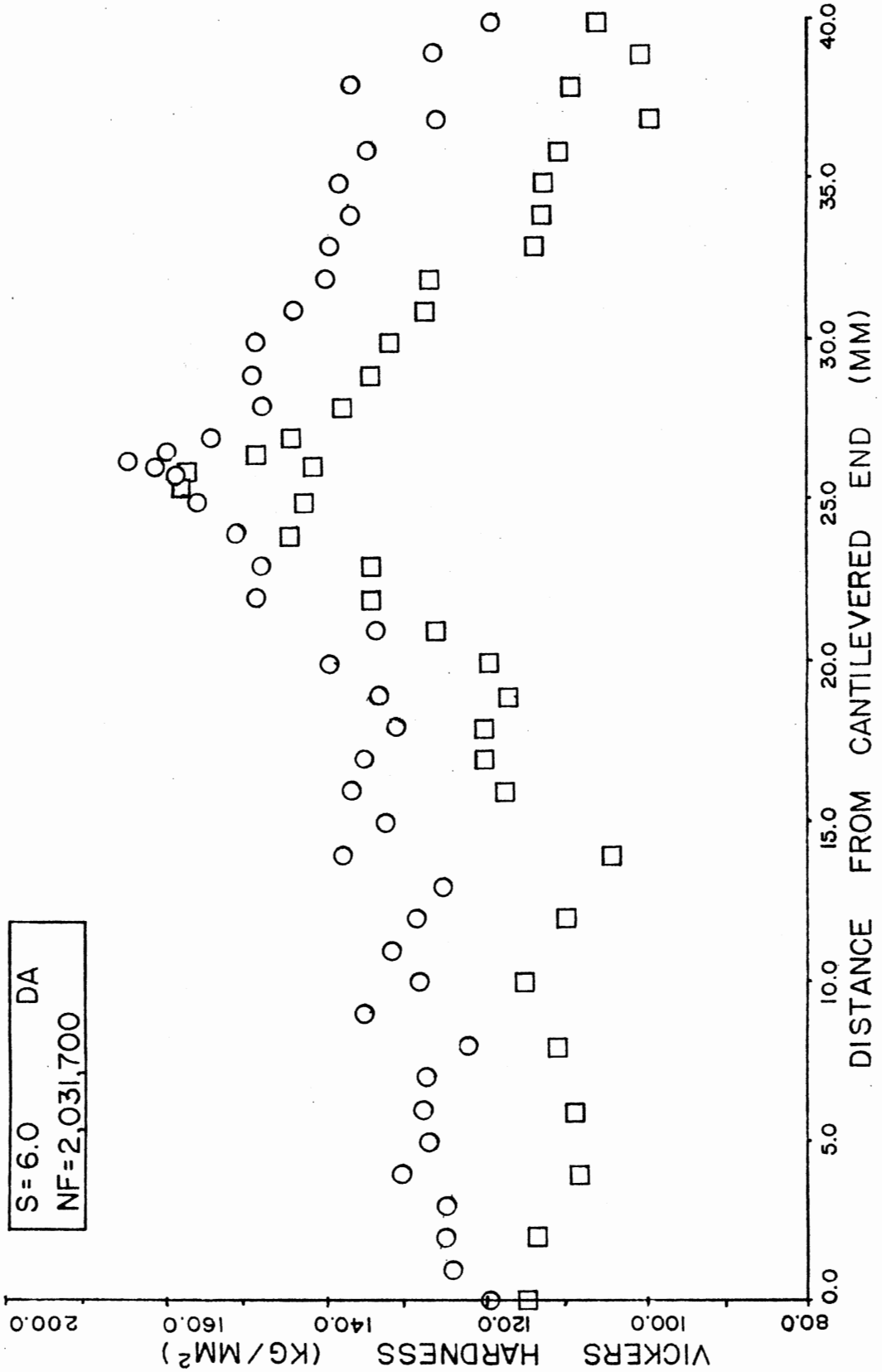
S=6.0 DA
NF=2,031,700
VICKERS HARDNESS (KG/MM²)
80.0
100.0
120.0
140.0
160.0
200.0
0.0
5.0
10.0
15.0
20.0
25.0
30.0
35.0
40.0
DISTANCE FROM CANTILEVERED END (MM)

Figure 13. Surface Hardness Profile of Sample 8B

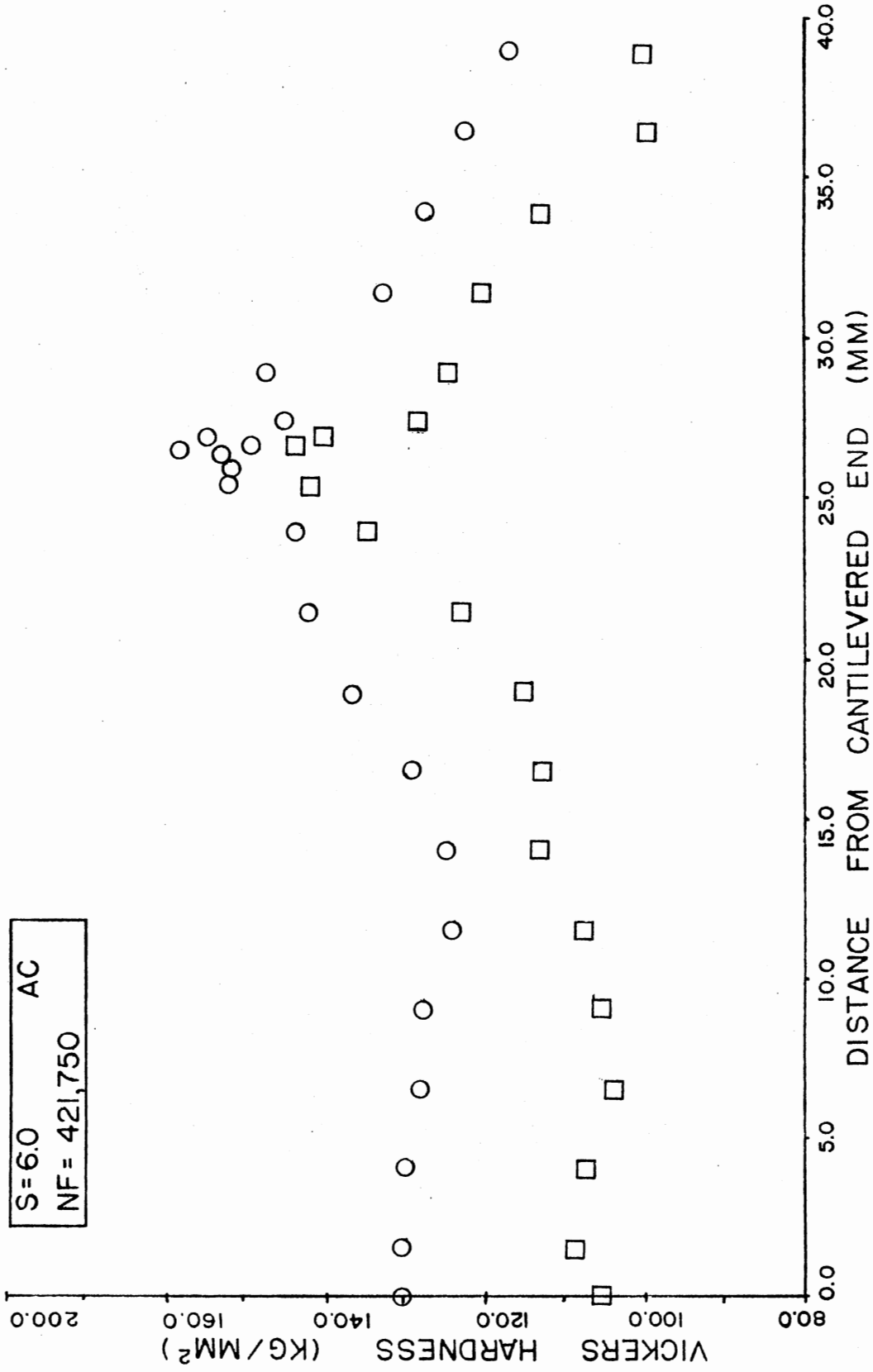
S=6.0 AC
NF= 421,750
VICKERS HARDNESS (KG/MM²)
80.0
100.0
120.0
140.0
160.0
200.0
0.0
5.0
10.0
15.0
20.0
25.0
30.0
35.0
40.0
DISTANCE FROM CANTILEVERED END (MM)

Figure 14. Surface Hardness Profile of Sample 6B

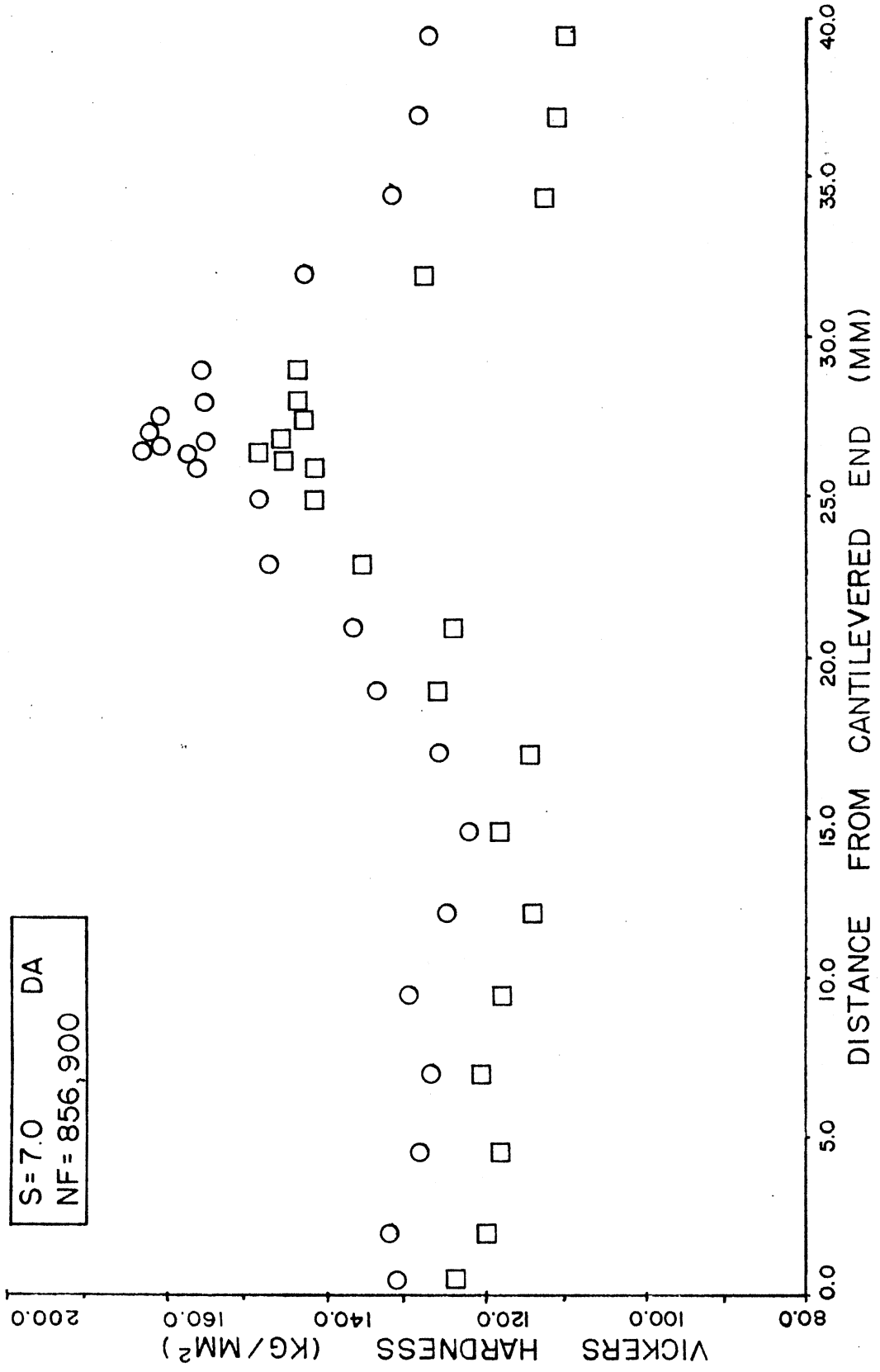
S=7.0 DA
NF=856,900
VICKERS HARDNESS (KG/MM²)
80.0
100.0
120.0
140.0
160.0
200.0
0.0
5.0
10.0
15.0
20.0
25.0
30.0
35.0
40.0
DISTANCE FROM CANTILEVERED END (MM)

Figure 15. Surface Hardness Profile of Sample 7B

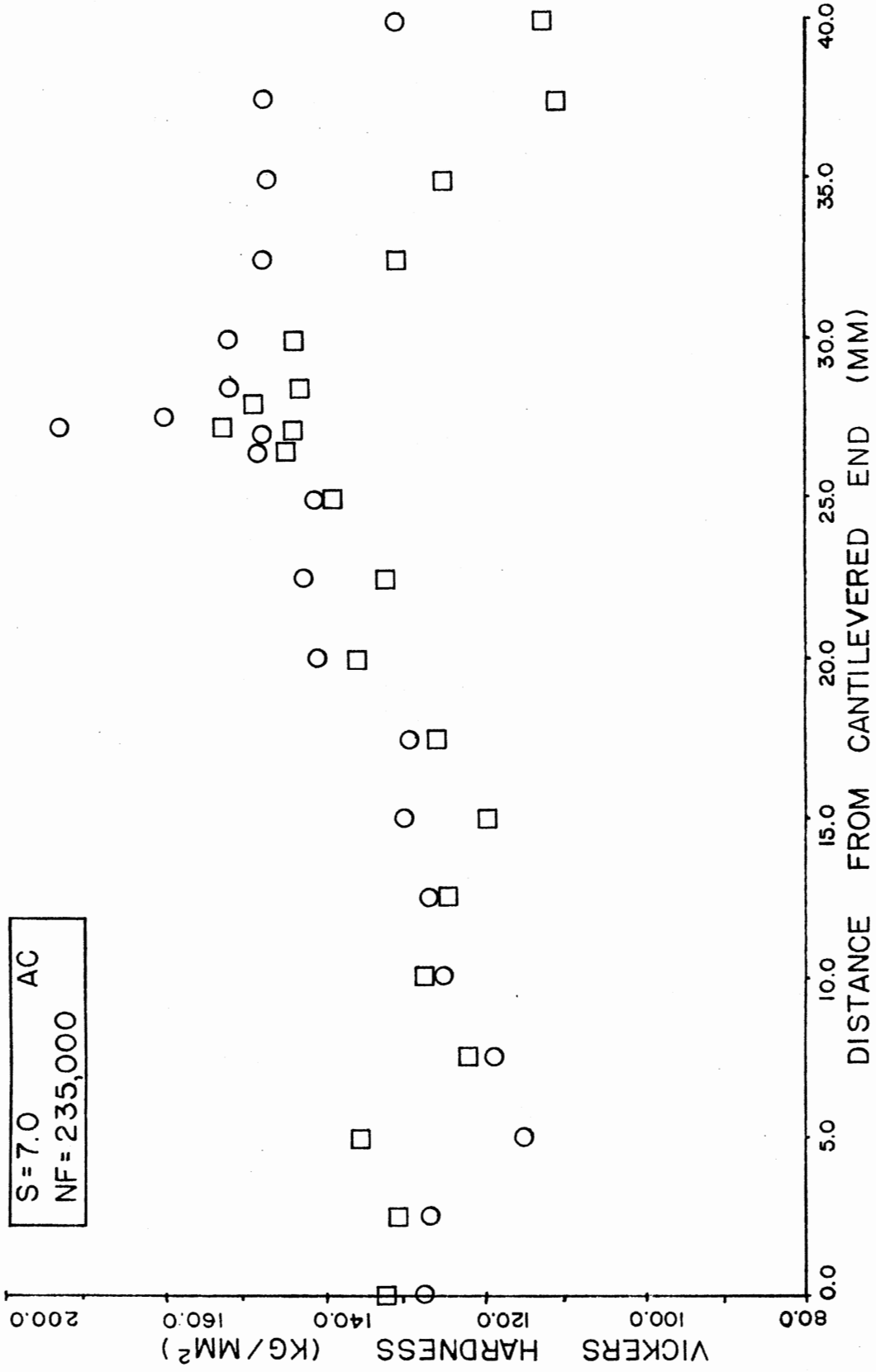
S=7.0 AC
NF=235,000
VICKERS HARDNESS (KG/MM²)
80.0
100.0
120.0
140.0
160.0
200.0
0.0
5.0
10.0
15.0
20.0
25.0
30.0
35.0
40.0
DISTANCE FROM CANTILEVERED END (MM)

Figure 16. Surface Hardness Profile of Sample 1A

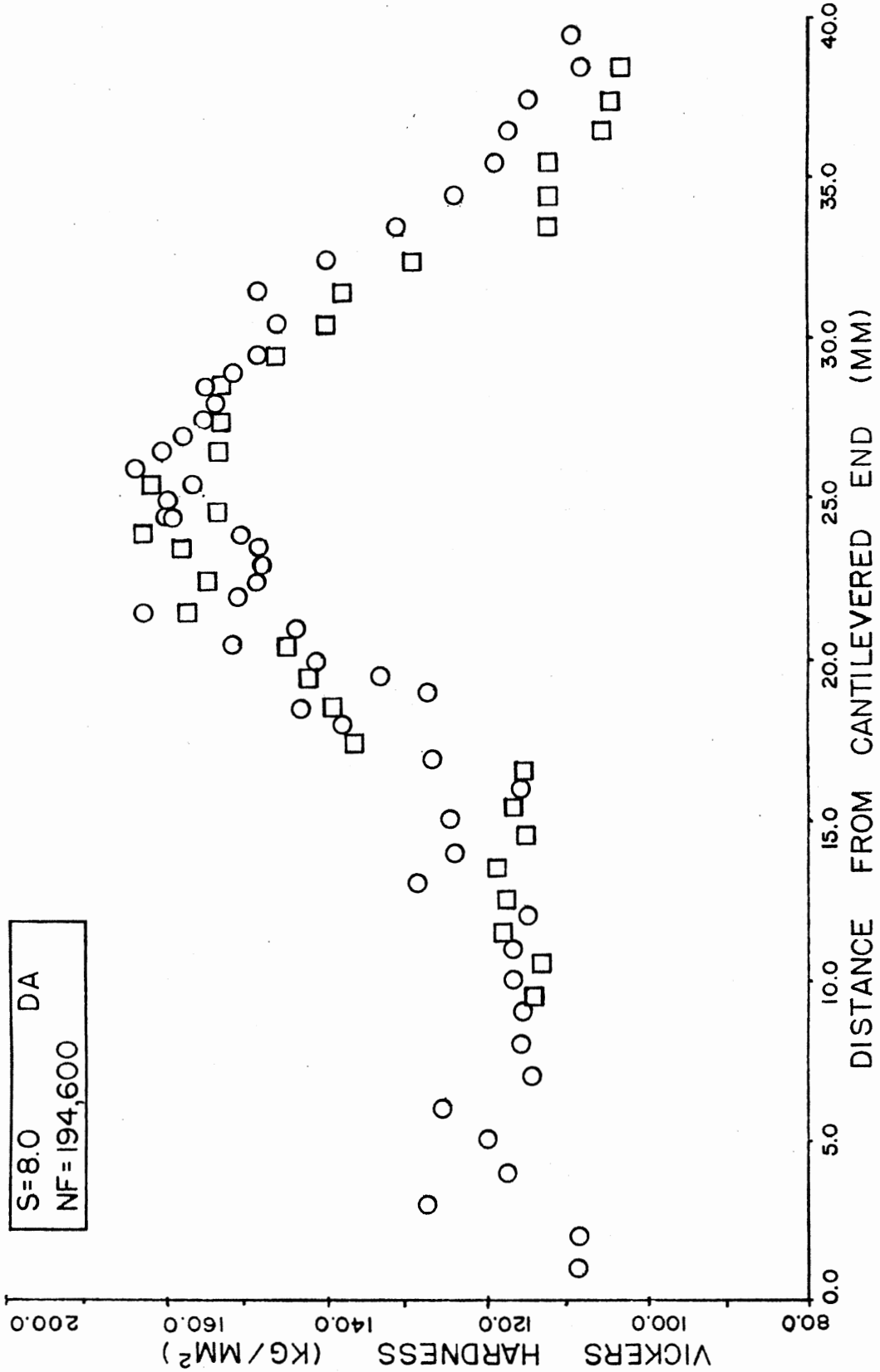
S=8.0 DA
NF=194,600
VICKERS HARDNESS (KG/MM²)
80.0
100.0
120.0
140.0
160.0
200.0
0.0
5.0
10.0
15.0
20.0
25.0
30.0
35.0
40.0
DISTANCE FROM CANTILEVERED END (MM)

Figure 17. Surface Hardness Profile of Sample 6A

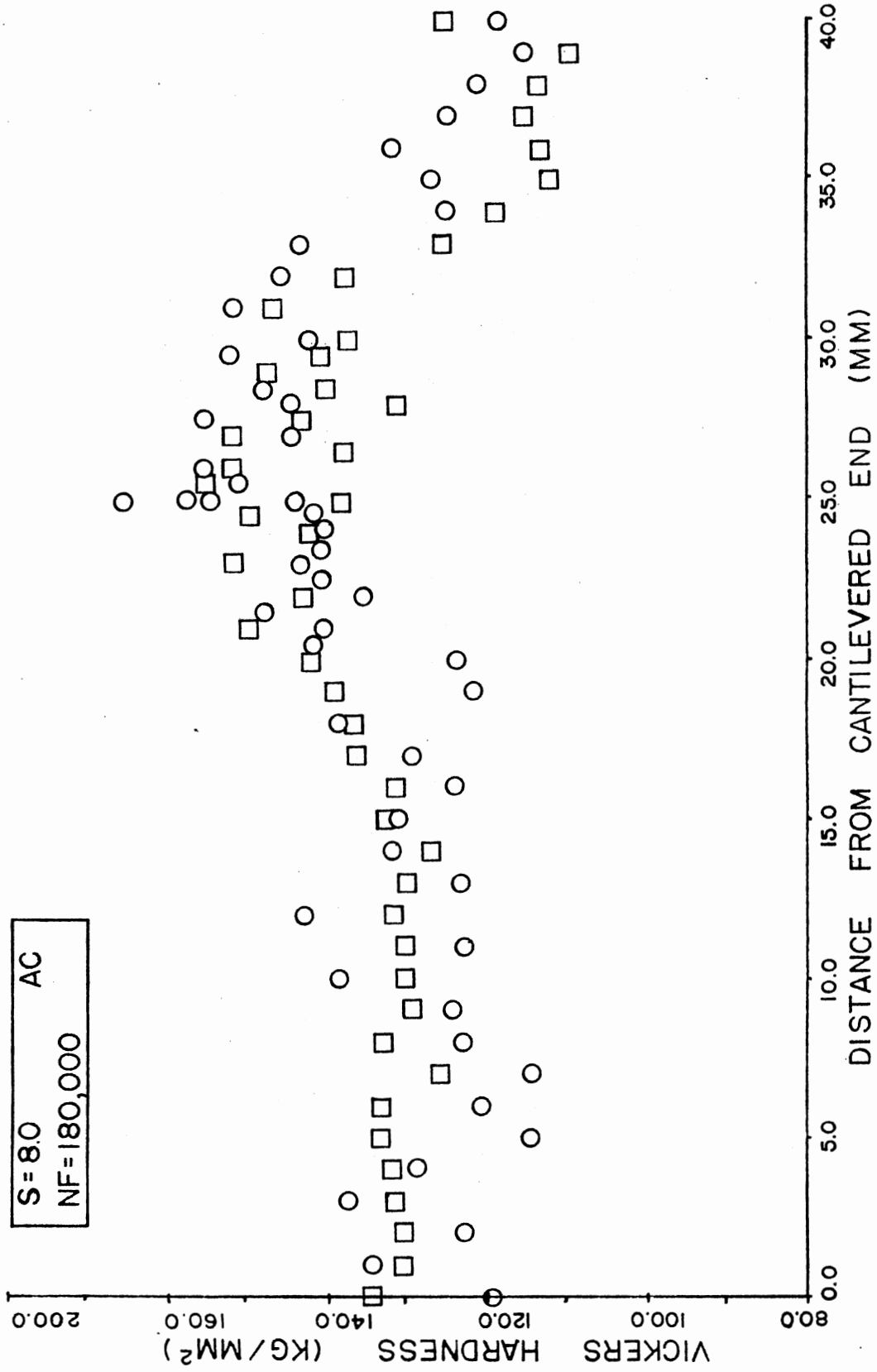
S=8.0 AC
NF=180,000
VICKERS HARDNESS (KG/MM²)
80.0
100.0
120.0
140.0
160.0
200.0
0.0
5.0
10.0
15.0
20.0
25.0
30.0
35.0
40.0
DISTANCE FROM CANTILEVERED END (MM)

Figure 18. Surface Hardness Profile of Sample 2A

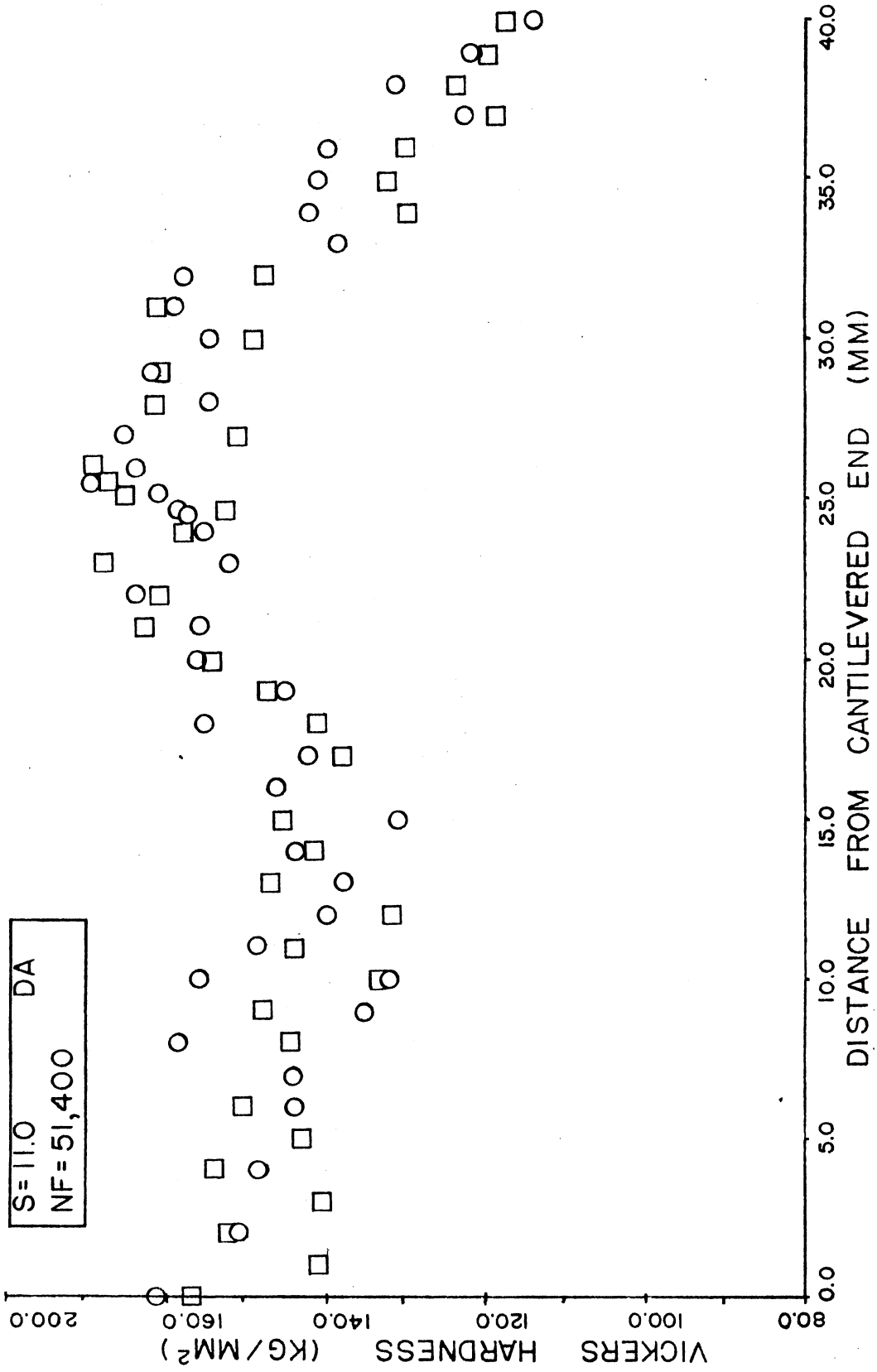
S=11.0 DA
NF=51,400
VICKERS HARDNESS (KG/MM²)
80.0
100.0
120.0
140.0
160.0
200.0
0.0
5.0
10.0
15.0
20.0
25.0
30.0
35.0
40.0
DISTANCE FROM CANTILEVERED END (MM)

Figure 19. Surface Hardness Profile of Sample 7A

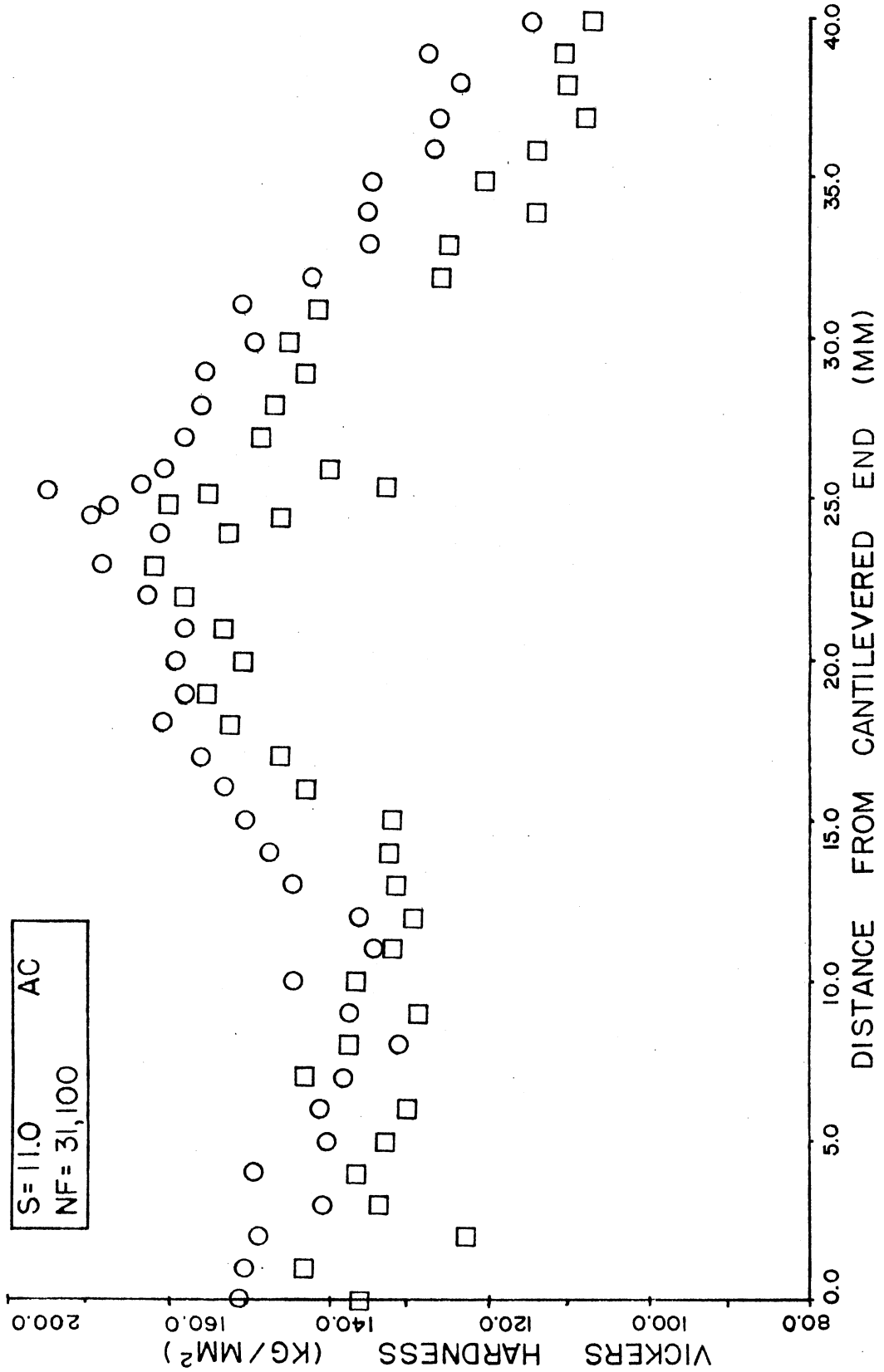
S= 11.0 AC
NF= 31,100
VICKERS HARDNESS (KG/MM²)
80.0
100.0
120.0
140.0
160.0
200.0
0.0
5.0
10.0
15.0
20.0
25.0
30.0
35.0
40.0
DISTANCE FROM CANTILEVERED END (MM)

Figure 20. Surface Hardness Profile of Sample 3A

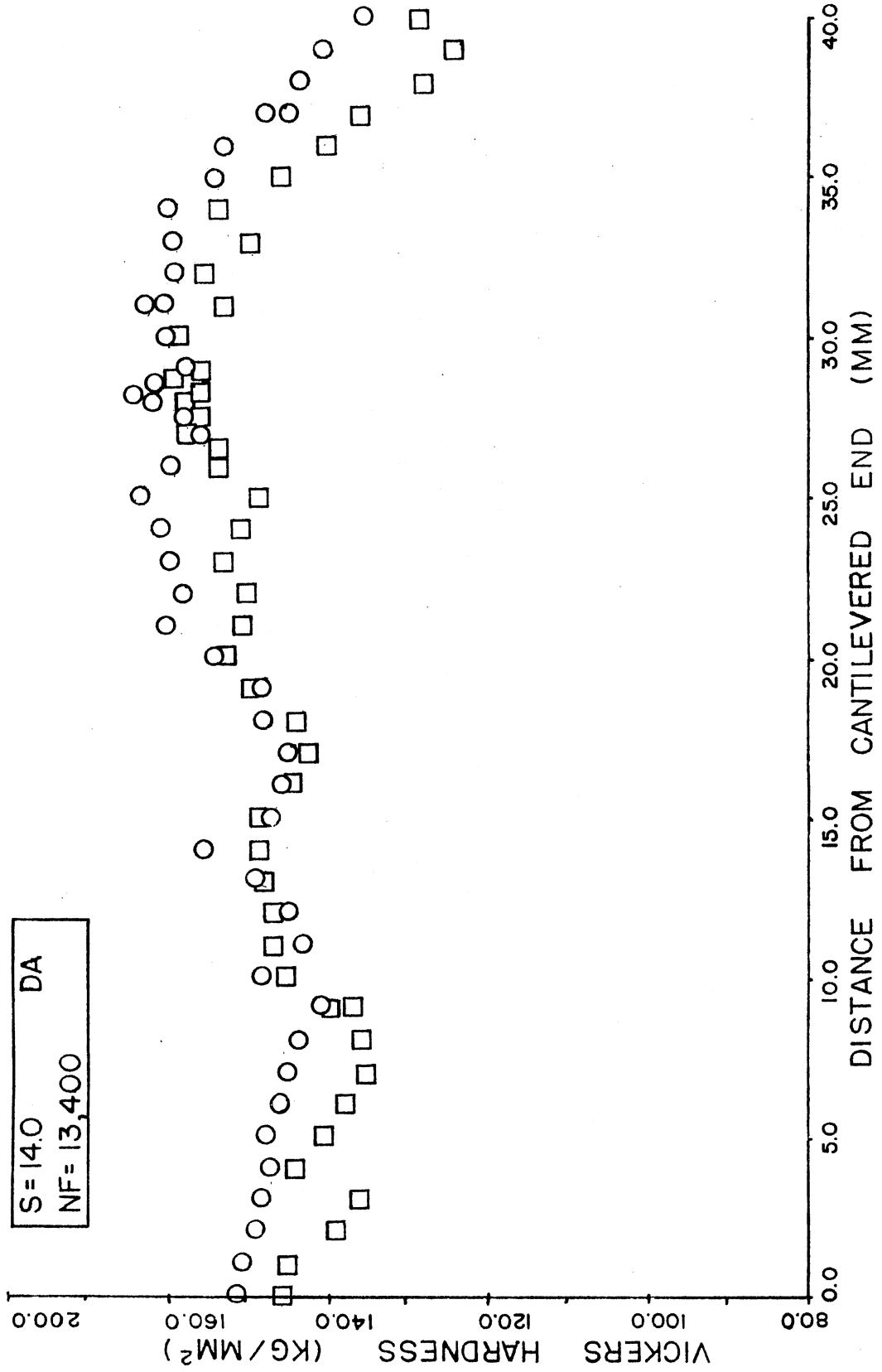
S=14.0 DA
NF=13,400
VICKERS HARDNESS (KG/MM²)
80.0
100.0
120.0
140.0
160.0
200.0
0.0
5.0
10.0
15.0
20.0
25.0
30.0
35.0
40.0
DISTANCE FROM CANTILEVERED END (MM)

Figure 21. Surface Hardness Profile of Sample 1B

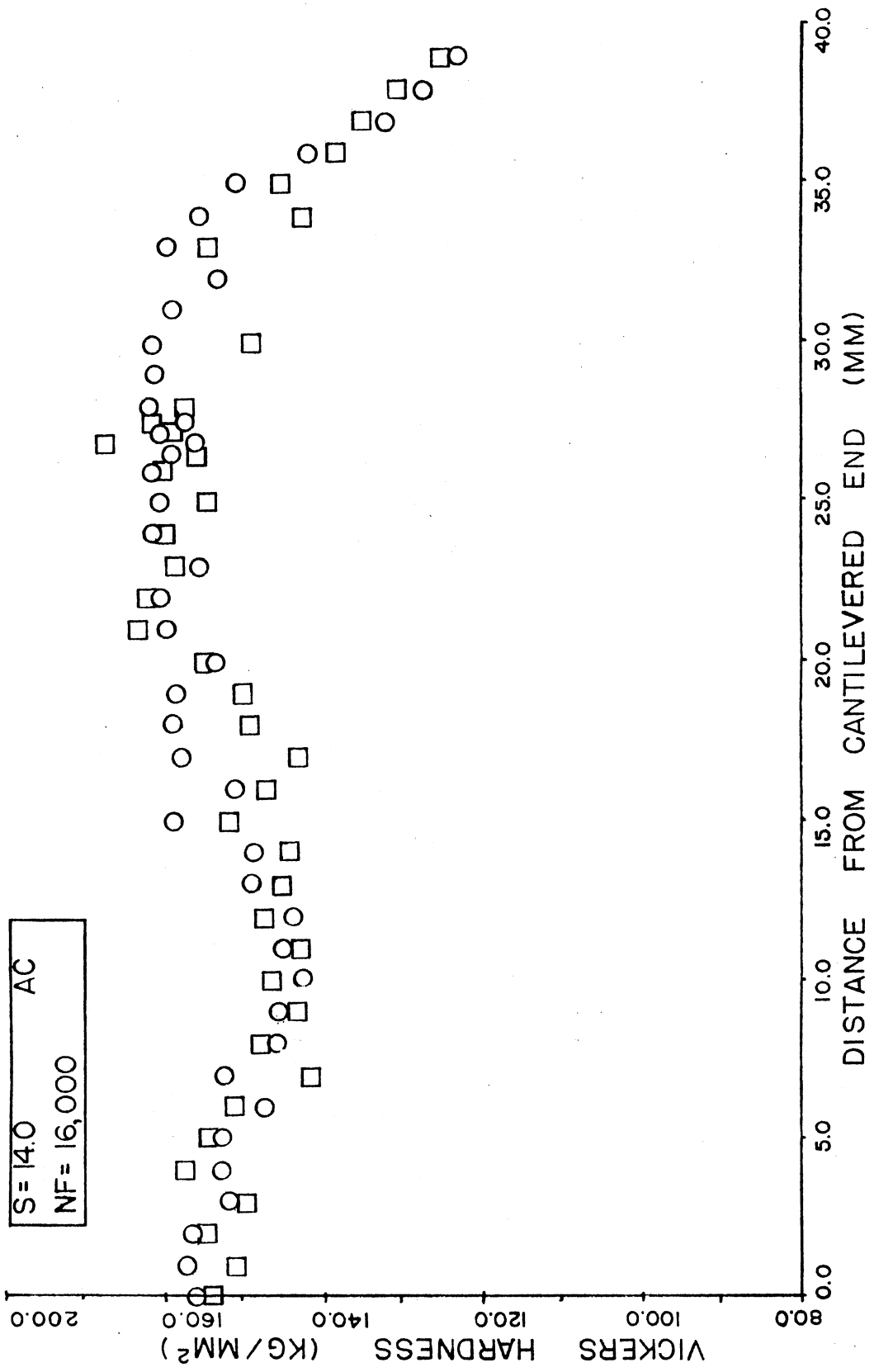
S= 14.0 AC
NF= 16,000
VICKERS HARDNESS (KG/MM²)
80.0
100.0
120.0
140.0
160.0
200.0
0.0
5.0
10.0
15.0
20.0
25.0
30.0
35.0
40.0
DISTANCE FROM CANTILEVERED END (MM)

Figure 22. Surface Hardness Profile of Sample 5B

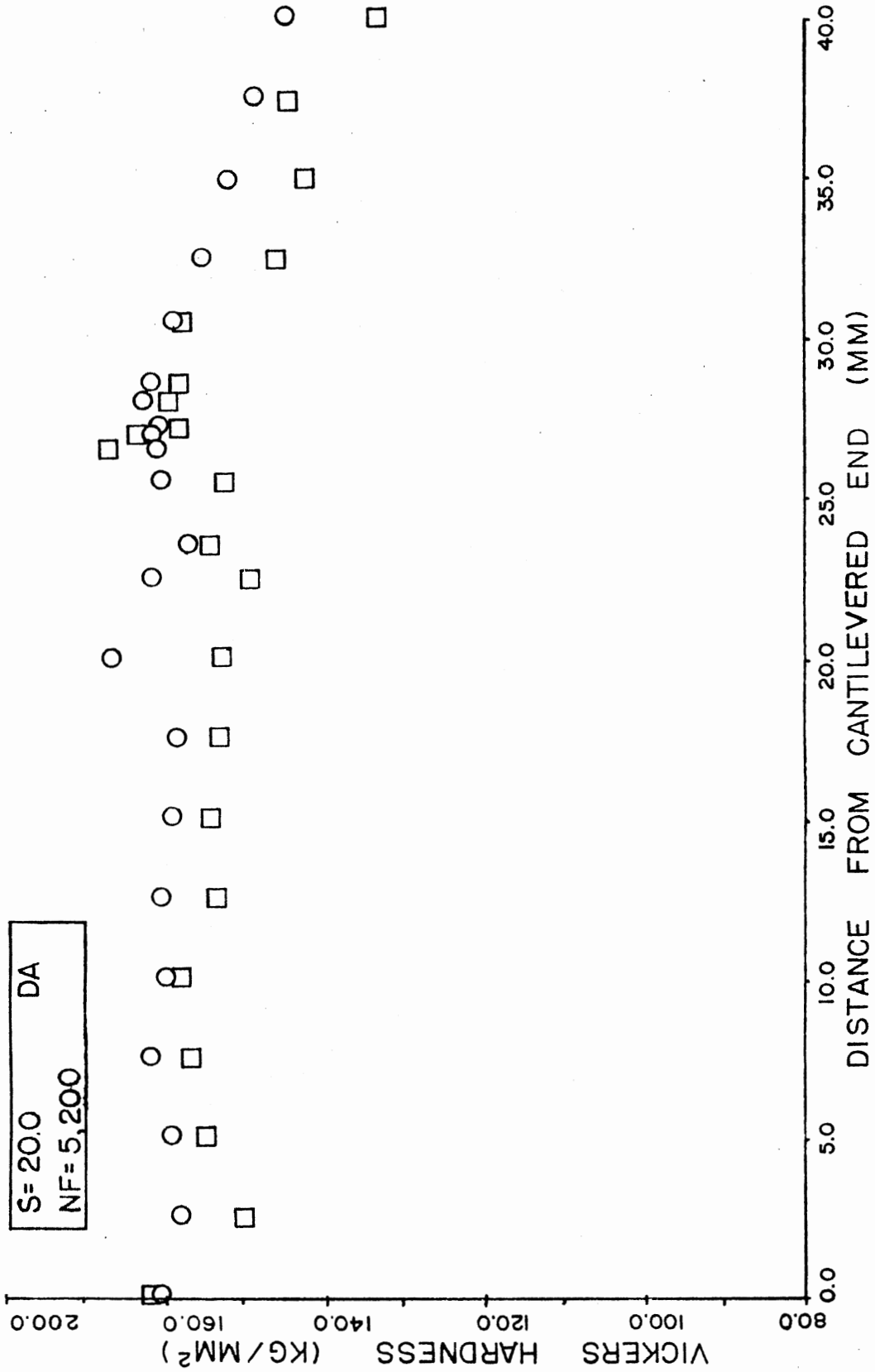
S= 20.0 DA
NF= 5,200
VICKERS HARDNESS (KG/MM²)
80.0
100.0
120.0
140.0
160.0
200.0
0.0
5.0
10.0
15.0
20.0
25.0
30.0
35.0
40.0
DISTANCE FROM CANTILEVERED END (MM)

It was observed that above a hardness value of $H_v \approx 140$, the hardness load was approximately the same for both indent loads. This can be observed in all the hardness profiles, Figures 10 through 22.

Optical observations were combined with hardness profiles to relate surface damage and hardness values. Slip lines were first noticed at a surface hardness of $H_v \approx 140$ for the two environments. Figures 23 and 24 show the first appearance of slip in the air and acid environments at an intermediate strain amplitude.

Surface deterioration in the two environments varied with the strain amplitude. In Figures 25 and 26, at a low strain amplitude, the acid environment specimen displayed gross damage due to corrosion. In Figures 27 and 28, at a high strain amplitude, surface damage is primarily due to plastic deformation and no difference was noticed between the two environments. It is suggested that amount of corrosion is highly dependent on time of test and that in the case of short fatigue lives, such as Figure 28, the environment had very little time to attack the surface.

As noted above, slip lines were first noticed by the optical microscope at a surface hardness of $H_v \approx 140$ kg mm^{-2} in both environments. The appearance of the slip, however, varied with the environments. Figures 23, 24, 29 through 32 show the progress of slip of an intermediate strain amplitude and the two environments. When the two environments were compared, slip was found to be more dispersed and somewhat more coarse in the acid environment. At high strain amplitudes there was only a slight difference between the environments, while at low strain amplitudes hardly any slip was visible due to corrosion, as shown in Figures 25 through 28.

Figure 23. First Appearance of Slip in a Dry Air Environment. Slip lines and/or cracks have appeared at the grain boundary at a surface hardness of $H_V \approx 140$ in a dry air environment. The texture of the grains is due to electropolishing. Sample 1A (X760)

Figure 24. First Appearance of Slip in a Corrosive Environment. Slip lines and/or cracks have formed through the grains. Notice how the slip line moves from the lower left to the upper right. The different appearance of the grains and twins is due to the corrosive environment. It appears that the amount of corrosive damage depends on the orientation of the grains. Surface hardness is $H_V \approx 140$. Sample 6A (X760)

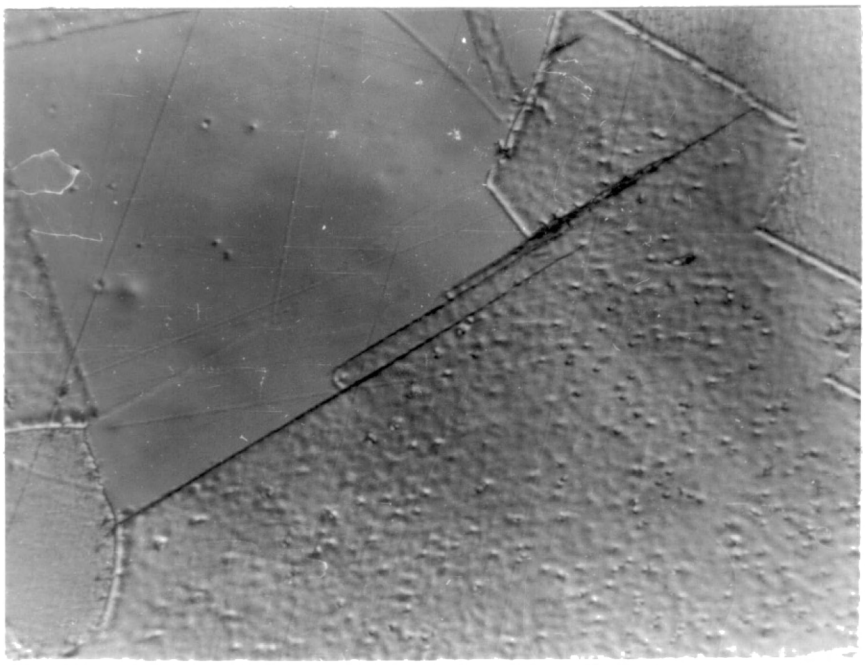

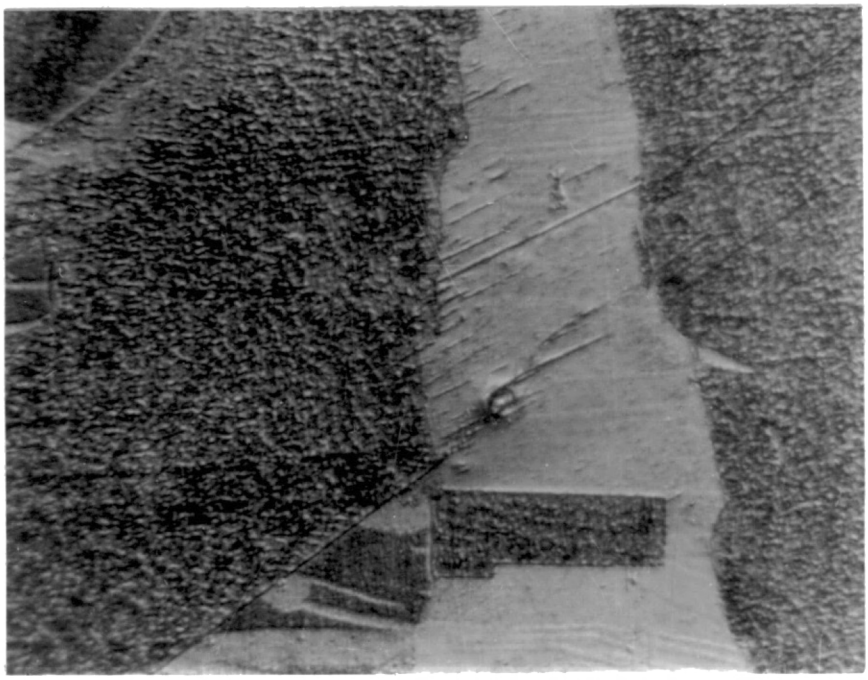

Figure 25. Low Strain Amplitude Fracture Surface in a Dry Air Environment. In the long fatigue life samples, the fracture edge has a distinct lack of gross surface deformation. Traces of slip are observed instead of distinct lines such as the crack along a grain boundary. Sample 4A (X380)

Figure 26. Low Strain Amplitude Fracture Surface in a Corrosive Environment. At the same strain amplitude as Figure 25, this sample has surface damage due to the corrosive environment. Though traces of slip are hard to find, a crack is seen at the middle to lower left. Sample 2B (X380)

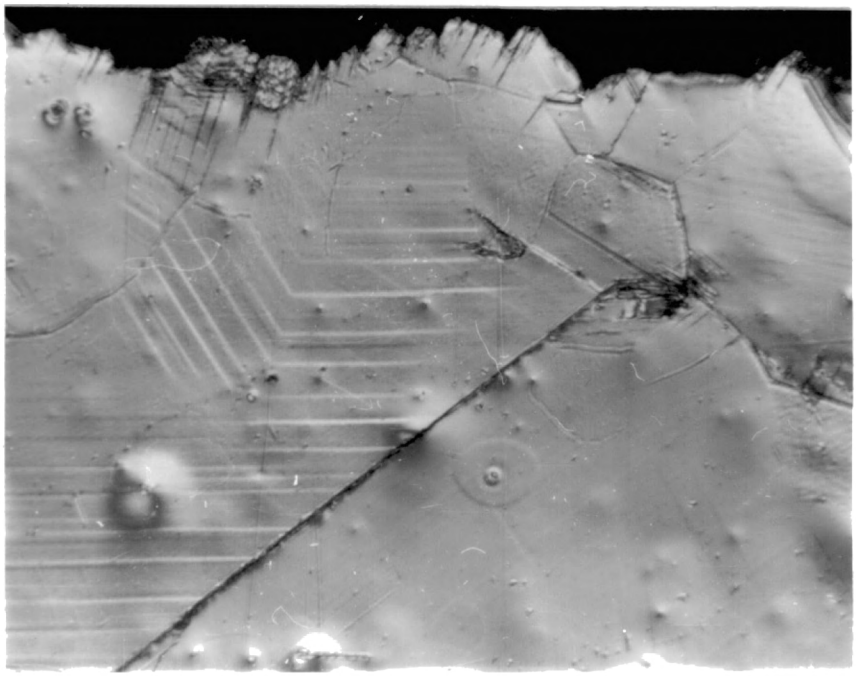

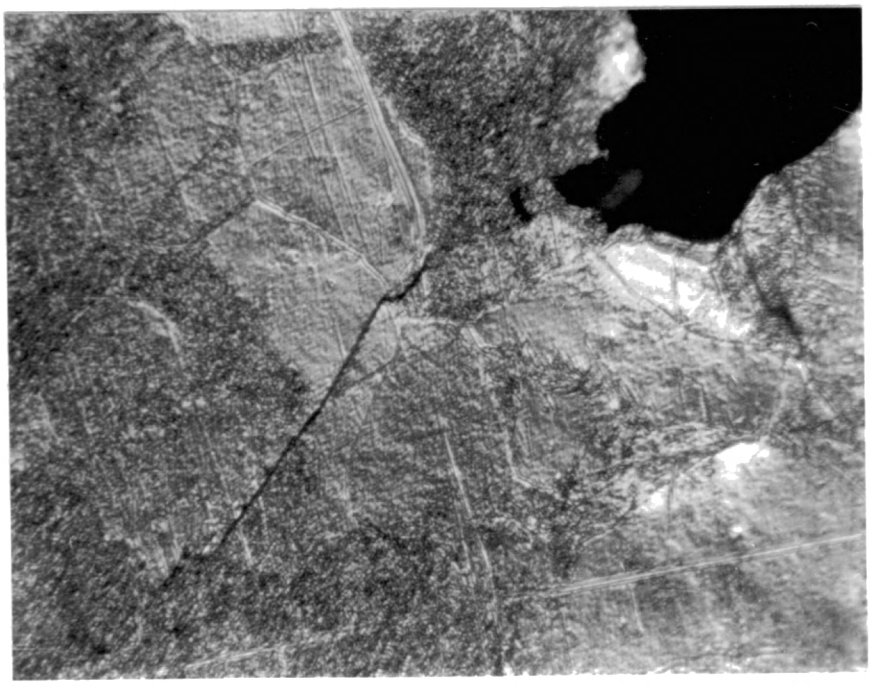

Figure 27. High Strain Amplitude Fracture Surface in a Dry Air Environment. In low cycle cycle fatigue the fracture surface has visible surface distortion with many grains having two or more slip directions. Sample 5B (X380)

Figure 28. High Strain Amplitude Fracture Surface in a Corrosive Environment. In low cycle fatigue the corrosive damage is not apparent. The slip lines tend to be wider and more coarse when compared to the slip in the dry air environment. Sample 9B (X380)

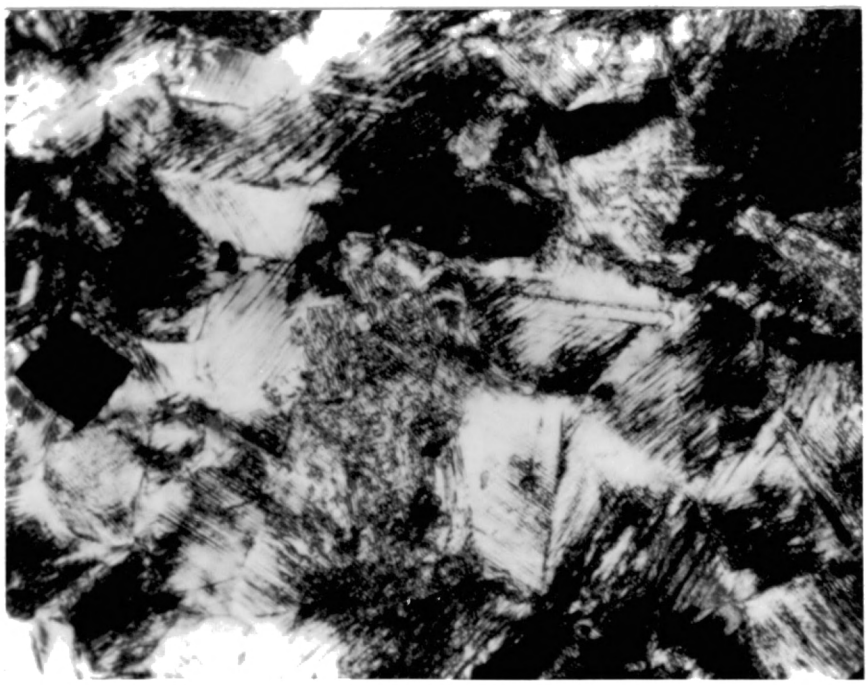

Figure 29. Progression of Slip in a Dry Air Environment. On the same sample as Figure 23, an area closer to the fracture edge is viewed to observe the progression of visible slip lines to a crack system. At a surface hardness of $H_V \approx 150$ some grains have multi-directional slip with slip lines and cracks connecting across grain boundaries. Sample 1A (X760)

Figure 30. Progression of Slip in a Corrosive Environment. On the same sample as Figure 24 the progression of slip to cracks is seen in an area of $H_V \approx 150$. The slip is mostly one-directional with the lines/cracks being more dispersed and somewhat more coarse than that in Figure 29. The crack is seen to travel from the lower left through a grain and along grain boundaries to the upper right. Sample 6A (X380)

Figure 31. Surface Damage in the Vicinity of the Limiting Surface Hardness in a Dry Air Environment. Persistent slip bands and extrusions/intrusions are seen in the middle grain surrounded by wavy slip. Cracking is through grains and along grain boundaries. Surface hardness is $H_V \approx 160$ and the location is adjacent to the fracture edge. Sample 1A (X380)

Figure 32. Surface Damage in the Vicinity of the Limiting Surface Hardness in a Corrosive Environment. Persistant slip bands and extrusions/intrusions are present but not as extensive as in Figure 31. Surface hardness is $H_V \approx 160$ and the location is adjacent to the fracture edge. Sample 6A (X380)

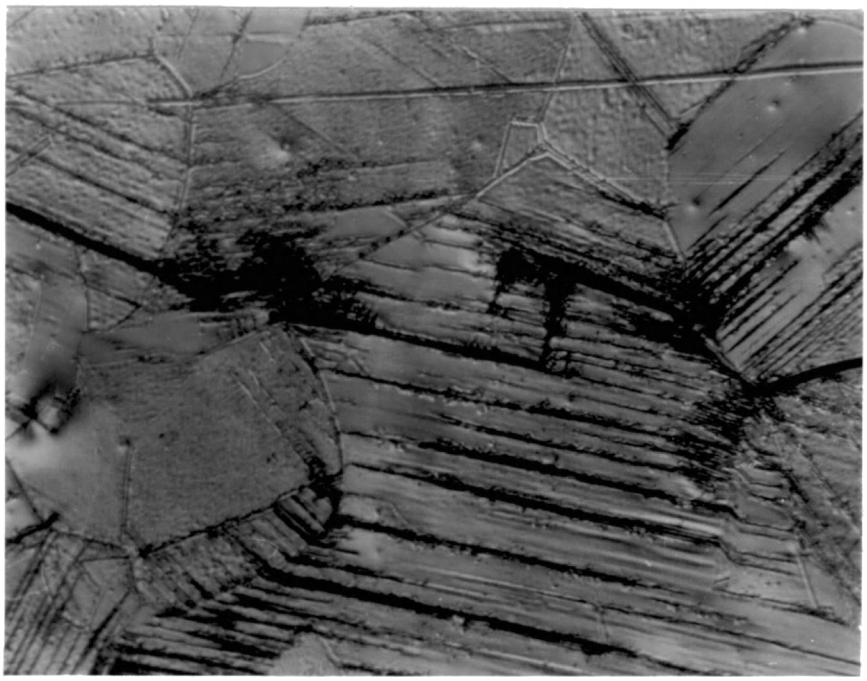

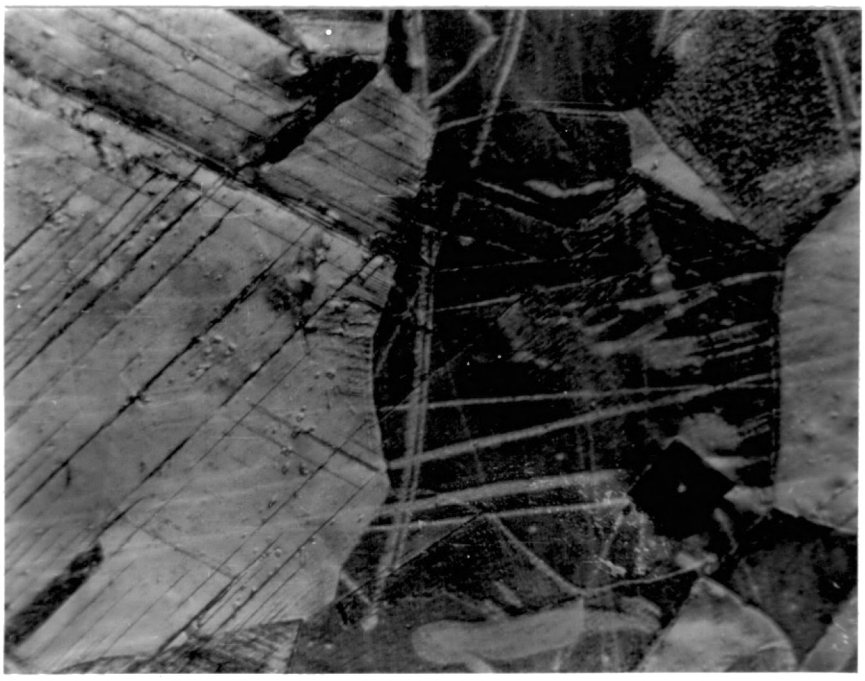

Strain amplitude also varied the appearance of the surface. Figures 33 through 36 show the extent of slip at the crack edge for a dry air environment at varying strain amplitudes. Grains exhibited slip only if oriented in the right direction for the slip system to work. In areas of higher strain amplitude, more than one slip system was activated and in some cases slip in three directions was observed, as shown in Figure 37. High strain amplitude also caused the persistent slip bands to broaden, as shown in Figure 38. This and the multiple cracking caused by a higher strain amplitude resulted in gross surface deformation.

Surface cracks were found to travel through the grains and along the grain boundary. As the strain amplitude was increased, more cracks were observed in the surface, as shown in Figure 39. Cracks were found to originate in the slip bands for both environments and all strain amplitudes. In a face-center cubic material there is little chance of grain boundary cracking due to the number of slip systems available.

The scanning electron microscope was used to identify surface cracks and extensive surface deformation. Incipient cracks were found in the region of $H_v \approx 140$ for both acid and dry air environments. Figure 40 shows a dry air environment sample with early cracking in slip lines through the grain boundaries. The SEM was also used to observe the areas of the maximum surface hardness ($H_v \approx 160$). Extensive intrusions and extrusions in this area are seen in Figure 41. Surface deformation of a surface crack at a high strain amplitude is shown in Figure 42.

One sample was lightly electropolished after fatigue fracture and is shown in Figure 43. The majority of the slip bands disappeared, although the persistent slip bands are visible as they reached deeper into the surface. Cracks were easily identified after electropolishing.

Figure 33. Fracture Edge of a Low Strain Amplitude Sample. Surface is clean and smooth as there are no traces of persistent slip bands and extrusions/ intrusions. Visible slip lines are only in the form of cracks in the surface. Sample 4A (X190)

Figure 34. Fracture Edge of a Low Strain Amplitude Sample. Slip bands are present in almost all grains and in some grains are multi-directional. Persistent slip bands and extrusions/intrusions are present but are not numerous. Surface is still smooth and somewhat clear. Sample 1A (X190)

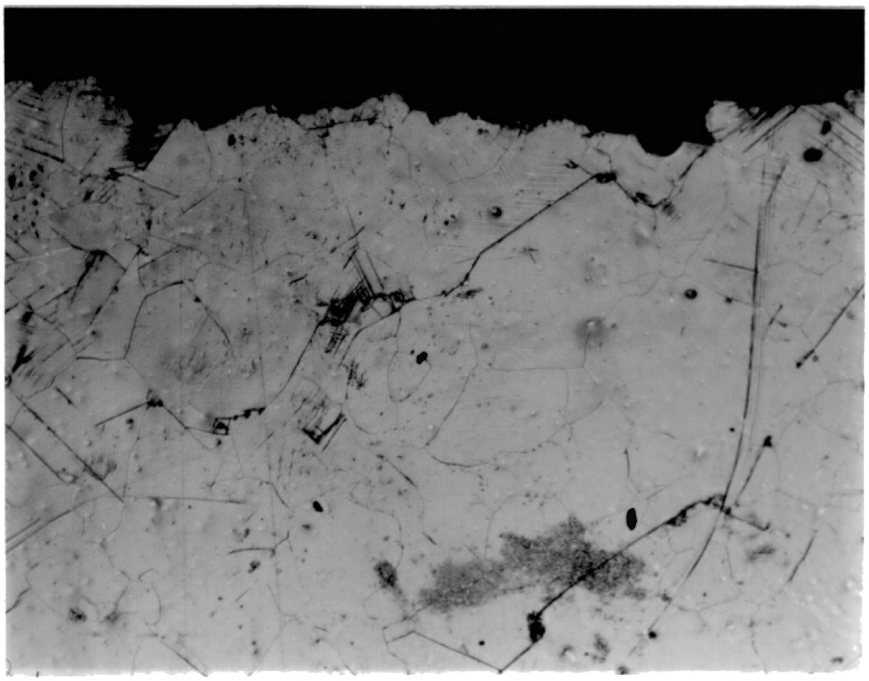

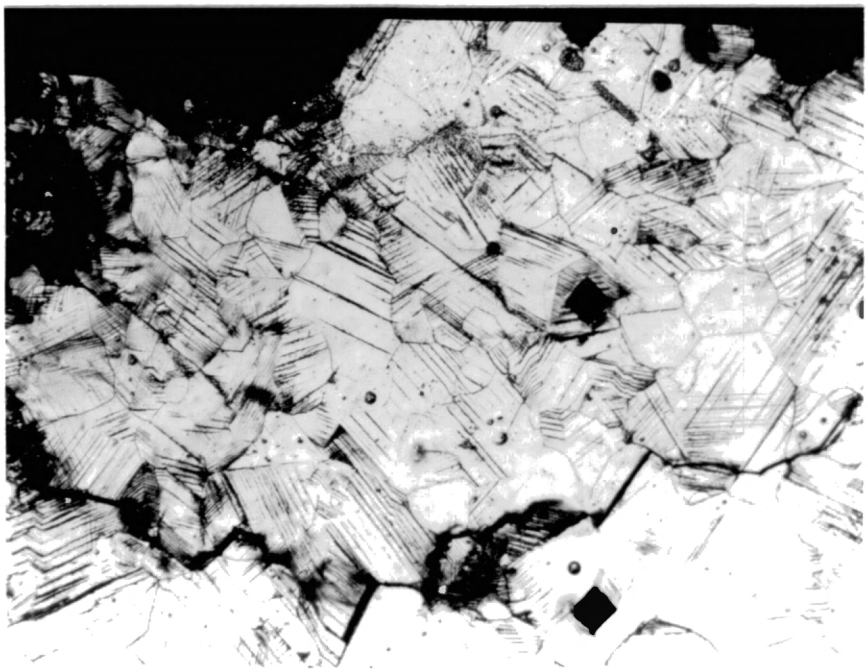

Figure 35. Fracture Edge of a High Strain Amplitude Sample. All grains at the edge have slip bands and intrusions/extrusions and most have slip in more than one direction. Surface is distorted around cracks in the surface and there the grain boundaries were very hard to discern. Sample 3A (X380)

Figure 36. Fracture Edge of a High Strain Amplitude Sample. All grains have multi-directional slip and surface distortions are quite extensive for an area some distance from the crack edge. Sample 5B (X190)

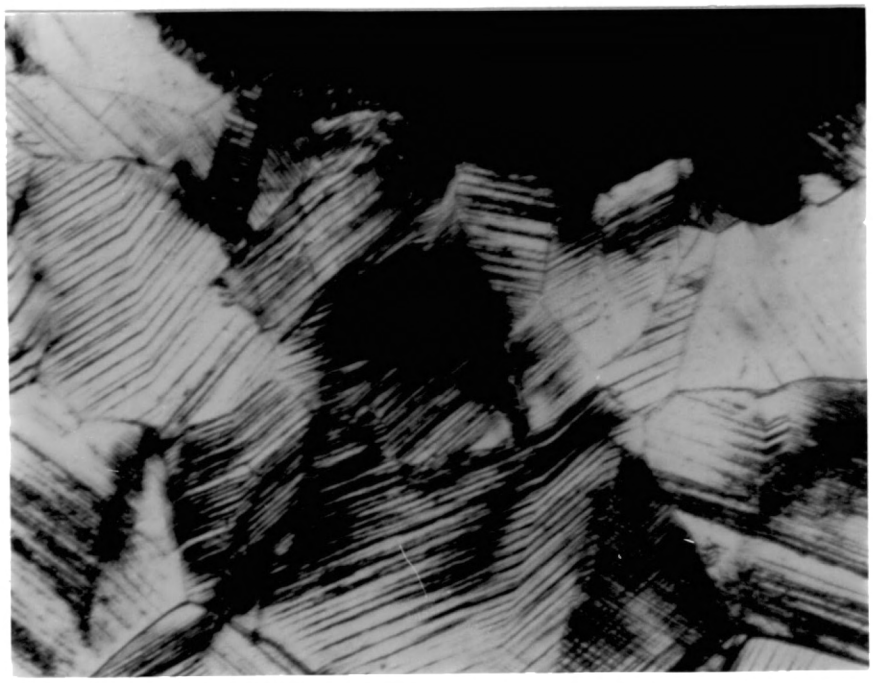

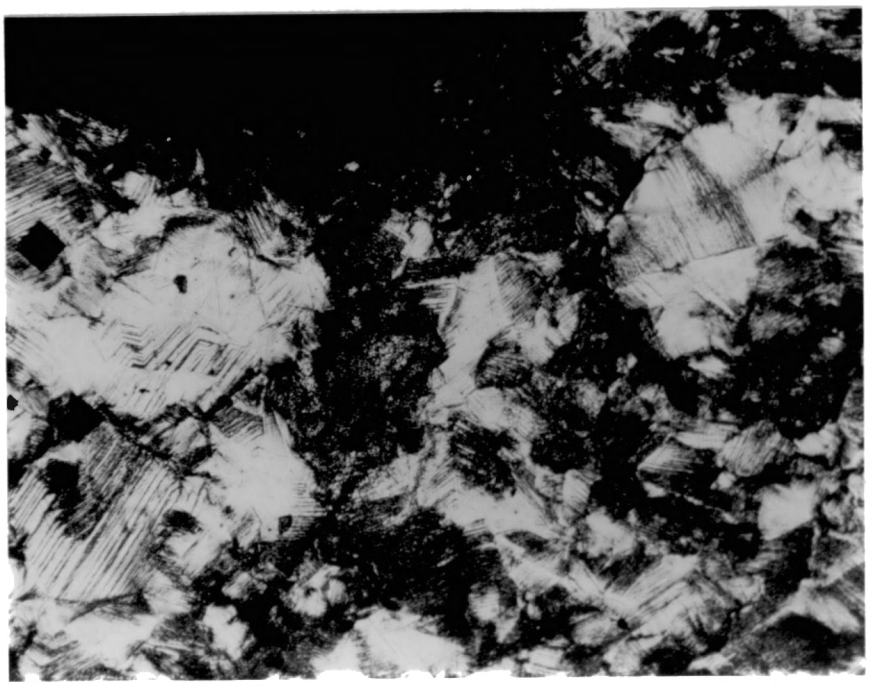

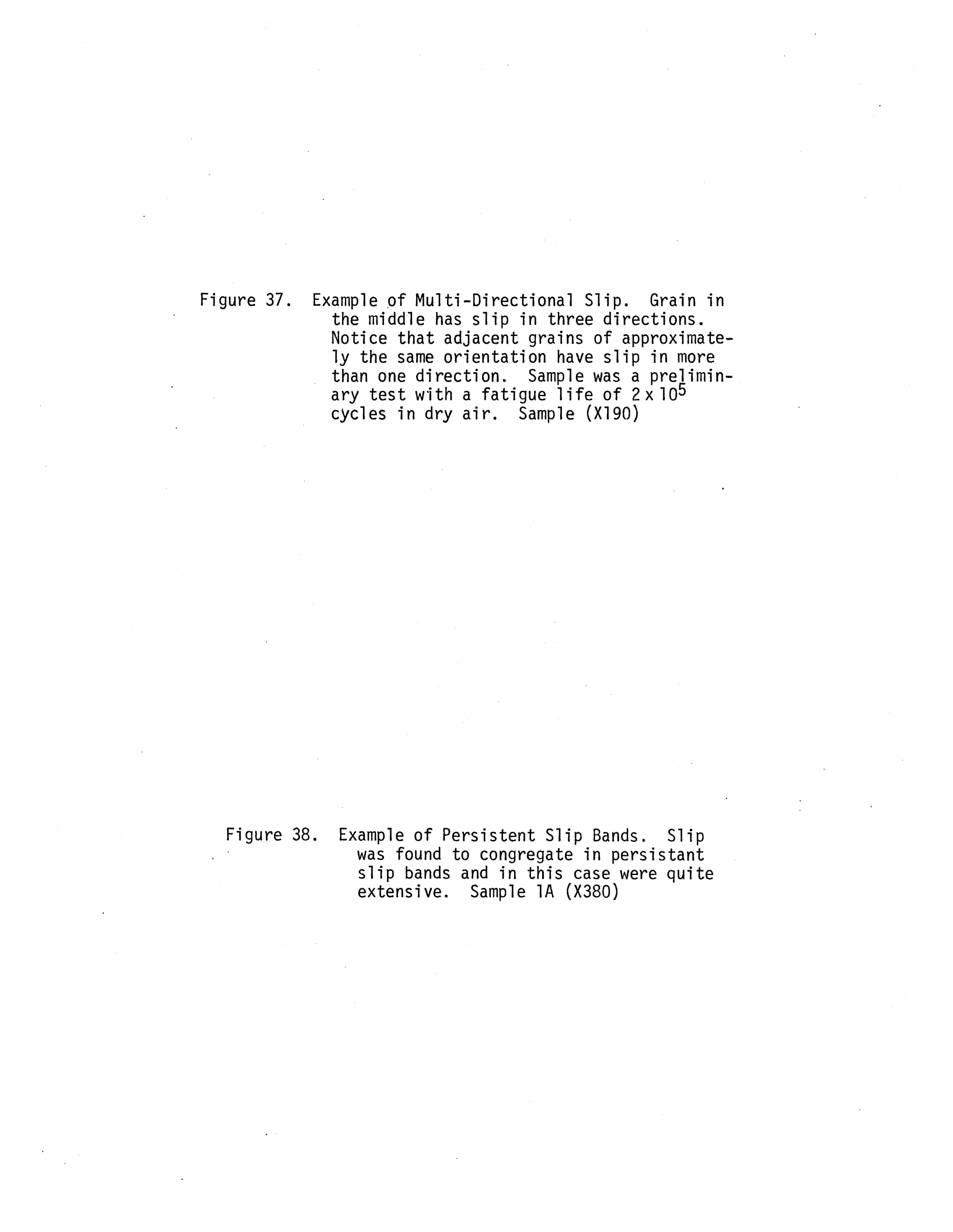

Figure 37. Example of Multi-Directional Slip. Grain in the middle has slip in three directions. Notice that adjacent grains of approximately the same orientation have slip in more than one direction. Sample was a preliminary test with a fatigue life of 2×10^5 cycles in dry air. Sample (X190)

Figure 38. Example of Persistent Slip Bands. Slip was found to congregate in persistant slip bands and in this case were quite extensive. Sample 1A (X380)

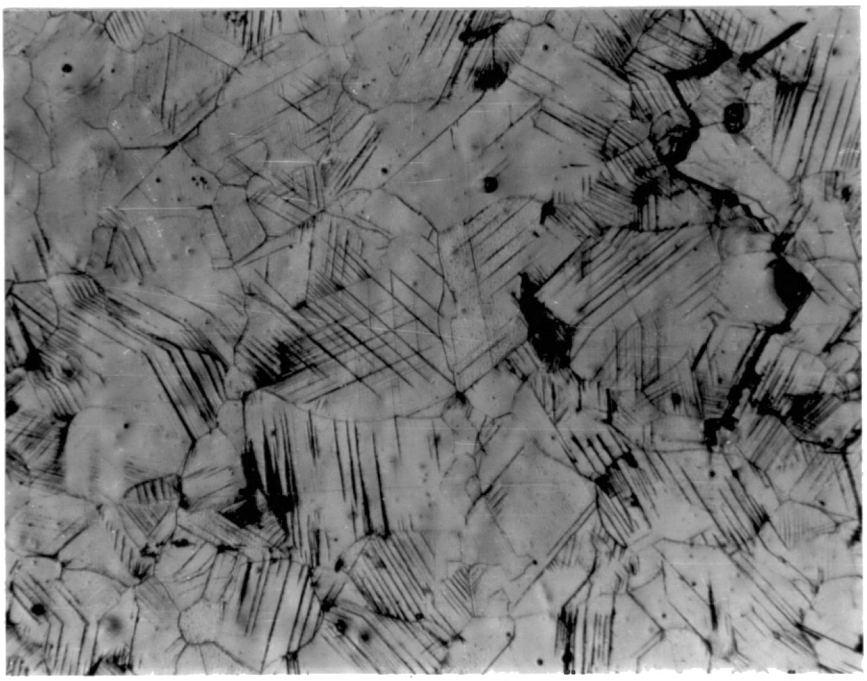

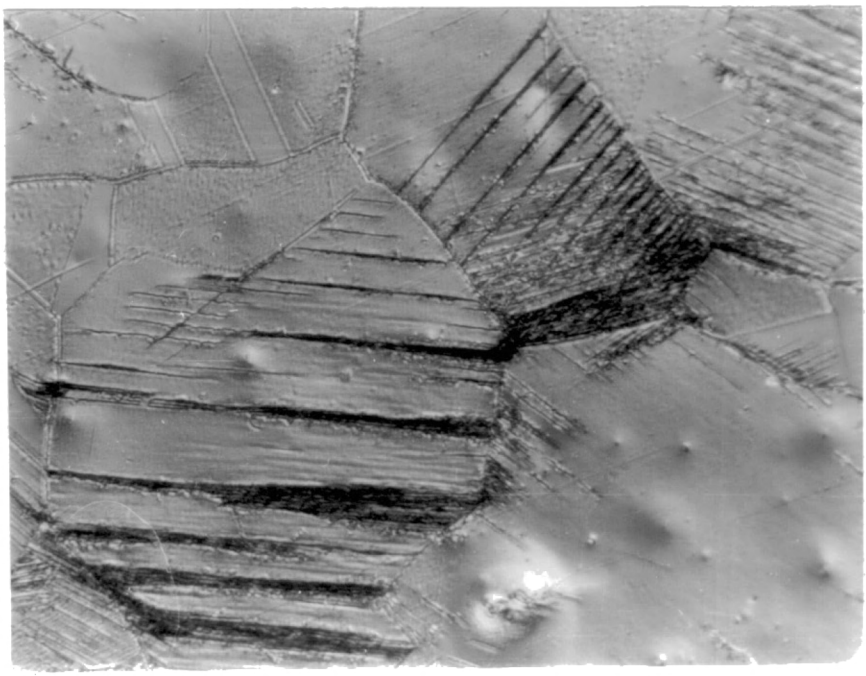

Figure 39. Stage I Crack Propagation. Cracking is in grains and along grain and twin boundaries. Sample is the same as in Figure 37 (X190)

Figure 40. Incipient Crack. A crack was found by use of the scanning electron microscope. Cracking is in grains and along grain boundaries. Surface hardness is $H_V \approx$ 143.6. Sample 6B (X1000)

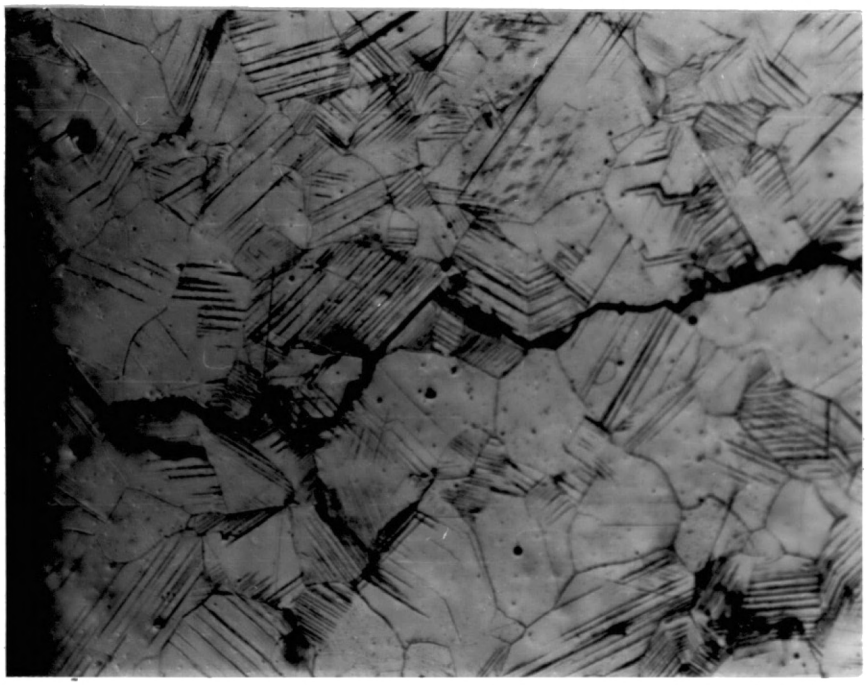

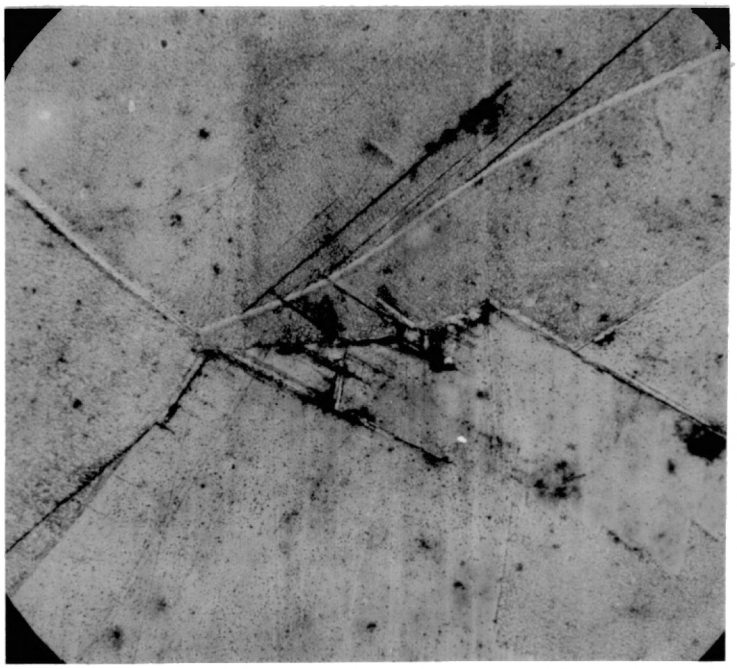

Figure 41. Extrusions in Two Directions. Extrusions occur when a thin film of material is shifted on the slip plane. Extrusions in two directions were observed with the scanning electron microscope. Sample 2A (X1200)

Figure 42. Tip of a Propagating Crack. This crack was observed to end/begin at the boundary of three grains. Much plastic deformation is present in the grains due to the high strain amplitude. Cracking is along crystallographic lines and in grain boundaries. Sample 2A (X1000)

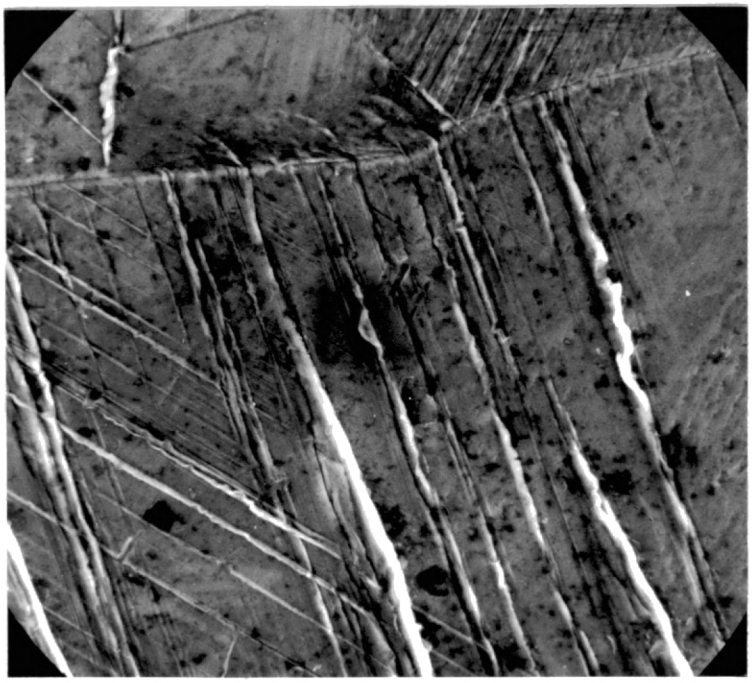

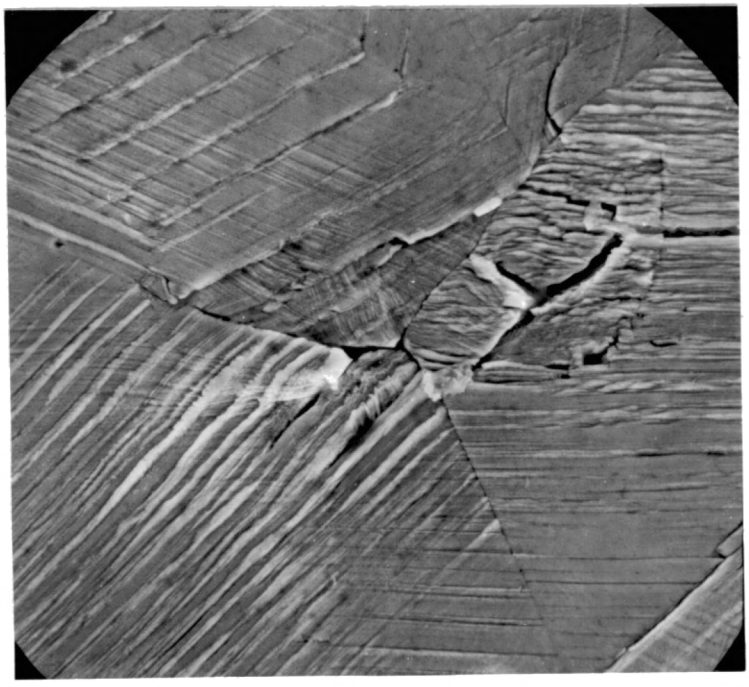

Figure 43. Sample Electropolished After Fatigue Failure. Cracks are exaggerated by electropolishing and seen above as dark thick lines. Dimpled lines are persistant slip bands. Light surface slip has been removed. Hardness here is $H_V \approx 155$ and was $H_V \approx 160$ before electropolishing. This was a preliminary sample tested in dry air with a fatigue life of 2×10^5 cycles (X380)

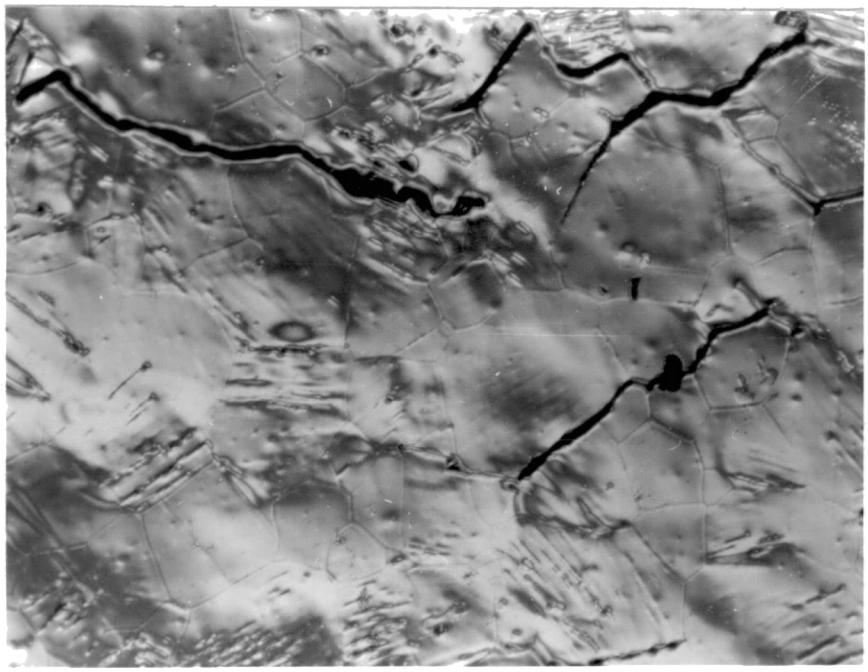

Discussion

From the test data it was found that the environment was indeed an important factor in the fatigue life for high cycle fatigue. At low cycle fatigue, no difference was found in the fatigue lives of the two environments. In low cycle fatigue the crack is initiated in the surface almost immediately and stage I crack propagation breaks the surface. A majority of the life (>90%) is spent in stage II crack propagation. It appears that from the test data, either the environment had little time to react with the surface or the environment does not affect stage II cracking. As the fatigue lives approached high cycle fatigue, it is seen that most of the life (>90%) is spent in stage I crack propagation with stage II occurring only when a critical section area exists. It can be inferred by the fatigue data gathered that the environment affected the stages of crack initiation and stage I crack propagation. Since in a high cycle fatigue cracks are known to initiate quite early (<10% of fatigue life), it could be inferred that the environment has the most effect on the stage I crack propagation.

Surface hardness profiles of two specimens with the same strain amplitude, the same indent load, and different environments were found to be similar, the significance that even though the environment resulted in a shorter life or an increased rate of fatigue, the magnitudes of the surface damage were the same. The appearance of cracks and slip bands were also similar in the two environments. As the extent of surface hardening and visible surface damage is the same, it can be inferred that the mechanism of crack initiation is independent of environment although the environment is responsible for increasing the rate of the fatigue

damage. This rate increase could be caused by a rate increase of surface hardening, a rate increase of stage I crack propagation, or a combination of both. In order to establish the extent of a rate increase in surface hardening, frequently interrupted fatigue tests must be done.

Evidence that initial cracking originated in slip bands was found for both high and low cycle fatigue lives. This suggests that the mechanism for crack initiation is also the same for all the strain amplitudes with the difference in high and low cycle fatigue being the extent of the final surface deformation. In order to establish this, interrupted fatigue tests are needed to follow crack initiation process in high and low cycle fatigue. The extent of the final surface deformation is a combination of surface hardness and microstructure appearance. In the environments tested and strain amplitudes for fatigue lives of 5×10^3 to 5×10^7 cycles, the maximum surface hardness was a constant value of $H_v \approx 160$. Continuing tests in high cycle fatigue are showing, however, that at an expected life of 2×10^8 cycles the final surface hardness may not reach that limiting hardness value.

In all samples in both environments, slip first appeared along the strain gradient at a hardness of $H_v \approx 140$. These areas were then observed with the scanning electron microscope for incipient cracks. It was demonstrated from those micrographs that where there was a slip line, there was a crack. It is noted that these cracks were not in extrusions/intrusions and persistent slip bands, as the traditional crack initiation model states. Also, the presence of slip and cracks at $H_v \approx 140$ disagrees with that model as the surface hardness did not reach the limiting hardness value before cracks were formed. These points, however, do agree with the work of Kramer (8). The practical application of cracks

forming at $H_v \approx 140$ is that when an annealed nickel part is subjected to cyclic strain, a microhardness test can be performed to find the extent of fatigue damage. If the hardness value is $H_v \approx 140$, then surface treatments such as mechanical polishing and electropolishing are needed to prevent the propagation of the cracks. The presence of cracks at $H_v \approx 140$ is confirmed for both environments and low strain amplitudes where most cyclic parts are strained. Confirmation for higher strains could be done by interrupted fatigue tests.

Surface hardness values above $H_v \approx 140$ were identical with different indent loads. This suggests that no strong surface layer exists as the surface has the same hardness as the subsurface. Also, by electropolishing only the very light slip from a fracture area, it was found that the hardness was the same as the initial fracture surface. This absence of a strong surface layer disagrees with Kramer's mechanism for crack initiation.

These results do tend to disagree in some aspects with both the traditional model and Kramer's model of crack initiation. Interrupted fatigue tests at high strain amplitudes are needed to verify the independence from strain amplitude of the results presented.

CHAPTER VI

CONCLUSIONS

1. A constant maximum surface hardness value ($H_v \approx 160$ kg mm^{-2}) occurs in the fatigue fracture zone. This value is independent of the test environment and independent of strain amplitudes with fatigue lives of 10^3 to 10^7 cycles.

2. Slip bands first appear at a constant surface hardness value ($H_v \approx 140$ kg mm^{-2}) independent of test environment.

3. In zones of visible slip, the surface hardness is constant to a depth of ten microns.

4. Fatigue cracks always initiate in slip bands independent of environment and strain amplitude.

5. Fatigue cracks initiate at a constant surface hardness independent of test environment.

BIBLIOGRAPHY

(1) Thompson, N., and N. J. Wadworth. "Metal Fatigue." Advances in Physics, 7 (1958), pp. 72-169.

(2) Laird, C., and D. J. Duquette. "Mechanisms of Fatigue Crack Nucleation." Corrosion Fatigue NACE-2, Houston, 1972, pp. 88-113.

(3) Grosskrentz, J. D. "The Mechanism of Fatigue I." Physica Status Solidi, 47 (1971), pp. 11-31.

(4) Grosskrentz, J. D. "The Mechanisms of Fatigue II, Fatigue Crack Initiation and Fatigue Crack Propagation." Physica Status Solidi, 47 (1971), pp. 359-396.

(5) Argon, A. S. "Effects of Surfaces on Fatigue Crack Initiation." Corrosion Fatigue NACE-2, Houston, 1972, pp. 176-181.

(6) Hertzberg, R. W. Deformation and Fracture Mechanics of Engineering Materials. New York: Wiley & Sons, 1976.

(7) Alden, J. H., and W. A. Backofen. "The Formation of Fatigue Cracks in Aluminum Single Crystals." Acta Metallurgica, 9 (1961), pp. 352-366.

(8) Kramer, I. R. "A Mechanism of Fatigue Failure." Metallurgical Transactions, 5 (1974), pp. 1735-1742.

(9) Achter, M. R. "Effects of Environment on Fatigue Cracks." Fatigue Crack Propagation, ASTM STP 415. Baltimore: American Society for Testing Materials, 1967, pp. 181-201.

(10) Duquette, D. J. "A Review of Aqueous Corrosion Fatigue." Corrosion Fatigue NACE-2, Houston, 1972, pp. 13-22.

(11) Kreiner, J. H. Internal Report. Oklahoma State University, Department of Mechanical and Aerospace Engineering, 1977.

(12) Nichols, H., and W. Rostoker. "Embrittlement of Steel by Organic Liquids." Environmental Sensitive Mechanical Behavior. New York: Gordon and Breach, 1966, pp. 213-238.

(13) Tegart, W. J. McG. The Electrolytic and Chemical Polishing of Metals. 2nd ed. New York: Pergamon Press, Inc., 1959.

(14) Beland, R. A. "Metallographic Techniques Used With Pure Nickel." Metals and Materials, 2 (1968), pp. 54-57.

(15) Davies, R. B., J. Y. Mann, and D. S. Kemsley. "Hardness Changes During Fatigue Tests on Copper." International Conference on Fatigue of Metals, IME-ASME, London, 1956, pp. 551-556.

(16) Coffin, L. F., and J. F. Tavernelli. "The Cyclic Straining and Fatigue of Metals." AIME Transactions, 215 (1959), pp. 794-817.

(17) Plumbridge, W. J., and D. A. Ryder. "The Metallography of Fatigue." Metals and Materials (August, 1969), p. 321.

(18) Wood, W. A. "Failure of Metals Under Cyclic Strain." International Conference on Fatigue of Metals, IME-ASME, London, 1956, pp. 531-537.

(19) Thompson, N. "Experiments Relating to the Basic Mechanism of Fatigue Tests on Copper." International Conference on Fatigue of Metals, IME-ASME, London, 1956, 527-530.

VITA

Josef Antonin Fila

Candidate for the Degree of

Master of Science

Thesis: A STUDY OF THE EFFECTS OF STRAIN AMPLITUDE AND ENVIRONMENT ON THE MECHANISM OF FATIGUE CRACK CONTROL IN NICKEL

Major Field: Mechanical Engineering

Biographical:

Personal: Born September 16, 1955, in Oklahoma City, Oklahoma, the son of Dr. and Mrs. L. J. Fila.

Education: Graduated from C. E. Donart High School, Stillwater, Oklahoma, in May, 1973; received the Bachelor of Science in Mechanical Engineering degree from Oklahoma State University in December, 1976; completed the requirements for the Master of Science degree at Oklahoma State University in May, 1978.

Professional Experience: Research assistant and graduate teaching assistant, Oklahoma State University, 1976-1977.

Professional Organizations: American Institute of Aeronautics and Astronautics, American Society of Mechanical Engineers, Pi Tau Sigma, Tau Beta Pi.